UNCLASSIFIED

AD NUMBER
AD903321
LIMITATION CHANGES
TO: **Approved for public release; distribution is unlimited.**
FROM: **Distribution authorized to U.S. Gov't. agencies only; Test and Evaluation; MAY 1970. Other requests shall be referred to Army Engineer Topographic Laboratories, Attn: ETL-TDL, Fort Belvoir, VA 22060.**
AUTHORITY
USAETL ltr, 28 Jan 1983

THIS PAGE IS UNCLASSIFIED

AD

Report Number FTR-1339-1

STEREO RADAR ANALYSIS

Final Technical Report

May 1970

Prepared for

U. S. Army Engineer Topographic Laboratories
Fort Belvoir, Virginia 22060

attn: ETL-TDL

Prepared by

Raytheon Company
Equipment Division
Autometric Operation
4217 Wheeler Avenue
Alexandria, Virginia 22304

Contract No. DACA76-69-C-0002 New

Sponsored by

Advanced Research Projects Agency
ARPA Order No. 1229

Destroy this report when it is no longer needed. Do not return it to the originator.

The findings in this report are not to be construed as an official Department of the Army position, unless so designated by other authorized documents.

14

Unclassified
Report No. FTR-1339-1
11 May 1970
12 96p.

9 FINAL TECHNICAL REPORT. Mar 69-Apr 70,

for

6 STEREO RADAR ANALYSIS.

15
Contract No. DACA76-69-C-0002, new

ARPA Order Number 1229 ARPA Order-1229

Program Code Number 8F40

Effective Date of Contract	-	12 March 1969
Contract Expiration Date	-	12 May 1970
Amount of Contract	-	$44,890

Contractor

Raytheon Company
Equipment Division
Autometric Operation
4217 Wheeler Avenue
Alexandria, Virginia 22304

Principal Investigator

Gordon Gracie
Raytheon/Autometric
703-751-1000 X337

Project Engineer

Frank Klimavicz
U.S. Army Engineer Topographic Laboratories
703-664-5814

10 Gordon Gracie,
Ronald K. Brewer,
John W. Bricker
Robert A. Johnson

048 020

1473

SUMMARY

The topographic accuracy of the AN/APQ-102(XA-2) side-looking radar and its specific applicability to 1:50,000 and 1:250,000 scale topographic mapping were tested using stereo radar techniques with real data. The two basic stereo configurations, opposite-side and same-side, were tested under various conditions relating to the data reduction technique, control, and image coordinate weighting. Also tested was the geometric fit of each individual radar record to the established ground control.

Although original plans called for a test area 25 nautical miles long by 4 nautical miles wide, shortcomings in the data actually acquired led to adoption of a much smaller test area. Moveover, lack of certain collateral data, such as range marks and time marks, required development of a special reduction technique based upon ground control in the test area.

Photogrammetric aerotriangulation of aerial photography flown simultaneously with the radar provided a means of defining the flight path. Ground points in the test area were also aerotriangulated, and used as control and as the standard for measuring radar accuracy.

The test results were surprisingly good, with the opposite-side stereo configuration providing the better accuracy. Average root mean square (RMS) values of 7.7 meters, 12.1 meters and 13.2 meters in X (across-track), Y (along-track) and Z (elevation), respectively, were obtained for the opposite-side case; corresponding RMS values of 9.5 meters, 20.0 meters and 16.7 meters were obtained for the same-side case. Results from fitting the individual radar records to the aerotriangulated positions also demonstrated excellent geometric fidelity in the radar imagery.

Although based upon limited data, the test results indicate that the AN/APQ-102(XA-2) radar, using stereo techniques, has much promise for all-weather, day-night mapping at scales of 1:50,000 and 1:250,000.

FOREWORD

This research was undertaken by the Autometric Operation of Raytheon Company. It was supported by the Advanced Research Projects Agency of the Department of Defense under ARPA Order No. 1229, and it was monitored by the U.S. Army Engineer Topographic Laboratories under Contract No. DACA76-69-C-0002, dated 12 March 1969.

This final report covers the period from March 1969 to April 1970. During the first months of the project, the Government was represented by Mr. Boyd E. Newman of the Engineer Topographic Laboratories. Later, the duties of Government Project Engineer were assumed by Mr. Frank Klimavicz, also of the Engineer Topographic Laboratories.

The project's Principal Investigator was Dr. Gordon Gracie of Autometric/Raytheon. Messrs. Eldon D. Sewell and Harl Hockeborn acted as in-house project consultants. Other Autometric/Raytheon personnel taking responsible part in the investigation were Messrs. Ronald K. Brewer, John W. Bricker and Robert A. Johnson.

TABLE OF CONTENTS

TABLE OF CONTENTS (Cont'd)

LIST OF ILLUSTRATIONS

LIST OF ILLUSTRATIONS (Cont'd)

LIST OF TABLES

1. INTRODUCTION

1.1 Background

Development of an all-weather, day-night mapping capability has long been a desired goal of the military mapping community. However elusive this particular capability may yet be, it is most likely to be achieved through use of side-looking airborne radar (SLAR). One radar system, the APQ-97(XE-1) high-resolution SLAR, has already been successfully applied to 1:250,000 scale topographic mapping of Darien Province, Panama, a perpetually cloudbound region of the earth.

After several generations of SLAR developm nt, there are now available a number of coherent side-looking radar systems which show much promise for all-weather, day-night mapping applications. The AN/APQ-102(XA-2) radar is one such system, and its application to medium and large scale topographic mapping, using stereo radar techniques, is the focal point of this investigation.

Many studies have already been undertaken to determine the theoretical feasibility of radar mapping. Radar image geometry and its differences from that of the central projection, error propagation, optimum flight line geometry, radar parallax, and equipment for stereo radar mensuration are some of the topics which have been recently investigated to give insight into the radar mapping problem. Little, however, has been done in the way of practical testing of real radar data in order to determine actual accuracy and develop useable techniques for data reduction. It is this particular aspect of the radar mapping problem which is addressed in this investigation.

This project was originally designed in anticipation of procuring a complete set of real data for investigation of mapping accuracies attainable from AN/APQ-102(XA-2) radar imagery under stereo conditions. Shortcomings in the data acquisition phase of the project resulted in an incomplete set of data which necessarily altered the course of the investigation. Following is a brief resume of the project's early history.

Effective date of contract was 12 March 1969. The original project plan stipulated SLAR imagery of a test area comprised of flat, rolling and mountainous terrain, to be acquired by the Government as soon as possible after contract initiation. In addition, vertical aerial photography, flown simultaneously with the radar, and also separately over the test area, was to be provided. This photography was to be taken with a cartographic camera, and some means was to be provided for time-correlating the simultaneous photography to the radar record. In April 1969, Autometric learned that much of the supporting data expected as input for the investigation would not be available. Specifically, there would be no time marks or range marks on the radar record, and no

correlating data between the cartographic camera exposures and radar record. Autometric was also notified by the Government that the test material would not be made available until after 1 June. The project work plan was revised to reflect the expected changes.

On 20 May, the Government Project Engineer requested Autometric to stop work on the project because of delays in data acquisition and uncertainty as to the nature of the data to be provided. Autometric agreed to this request, and no further work was done until 18 September, when the radar imagery and supporting data were finally received from the Government. A further revision of the project work plan was then made to accommodate the actual data, as received, and the contract expiration date was extended to 12 May 1970, in accordance with the delay experienced in receiving the data.

The incompleteness of the acquired data made it quite evident that some "bootstrapping" would have to be done to establish the missing information. Although it was expected that such "bootstrapping" would affect the results (and perhaps their validity) to some extent, it was believed that useful information could still be derived from the investigation. The actual results later obtained indeed bore this out.

1.2 Objective

The objective of this investigation is to determine the accuracy with which topographic map information can be extracted from specific stereo imagery obtained from the AN/APQ-102(XA-2) radar, and in particular to determine the applicability of the AN/APQ-102(XA-2) radar to 1:50,000 and 1:250,000 scale topographic mapping.

1.3 Test Material

Radar imagery and supporting aerial photography were acquired by the 4416th Test Squadron of the USAF Tactical Air Reconnaissance Center (TARC), located at Shaw Air Force Base, South Carolina.

The original flight plan specified coverage of a target area, 25 nautical miles long by 4 nautical miles wide, in the locality of Atlanta, Ga.; Chattanooga, Tenn.; or Knoxville, Tenn.; the final area selection being dependent on weather and air space availability.

Data acquisition was to be conducted in two parts under the following specifications:

Part 1: High Altitude

Sensors:	AN/APQ-102(XA-2) Side-Looking Radar KC-1B Mapping Camera (stabilized) KS-72 3-inch Vertical Camera
Altitude:	30,000 feet Above Ground Level (AGL)
Airspeed:	420 knots
SLAR Mode:	3 (optimum side)
Offset:	6 nautical miles (NM) from near edge of target area.
Passes:	Two passes on each side of the target in race track pattern.

Part 2: Low Altitude

Sensors:	Same as Part 1
Altitude:	5,000 feet Above Ground Level (AGL)
Airspeed:	Same as Part 1
SLAR Mode:	Same as Part 1
Offset:	6 nautical miles (NM) and 8 nautical miles (NM) from near edge of target area.
Passes:	Two passes at each offset distance on one side of the target area.

In addition, one aerial photographic run at 5,000 feet AGL and 420 knots was planned over the target area centerline, using only the KC-1B and KS-72 cameras (i.e., no radar).

The flight plan was amended to include one additional mission, a pass flown at 30,000 feet AGL and 420 knots, offset 18 NM from the near edge of the target area, and operating in SLAR Mode 4.

The flight configuration, as planned, is shown in Figure 1. General instructions required that all passes be parallel (within one degree) with each other and with the centerline of the target area, and that cloud cover be 10% or less.

The area actually flown for the test was the one located near Atlanta, Georgia, as shown in Figure 2. Radar imagery and aerial photography for Sorties 08-61, 08-75 and 08-212, flown on 8 August, 11 August and 26 August 1969, respectively, were supplied for the investigation.

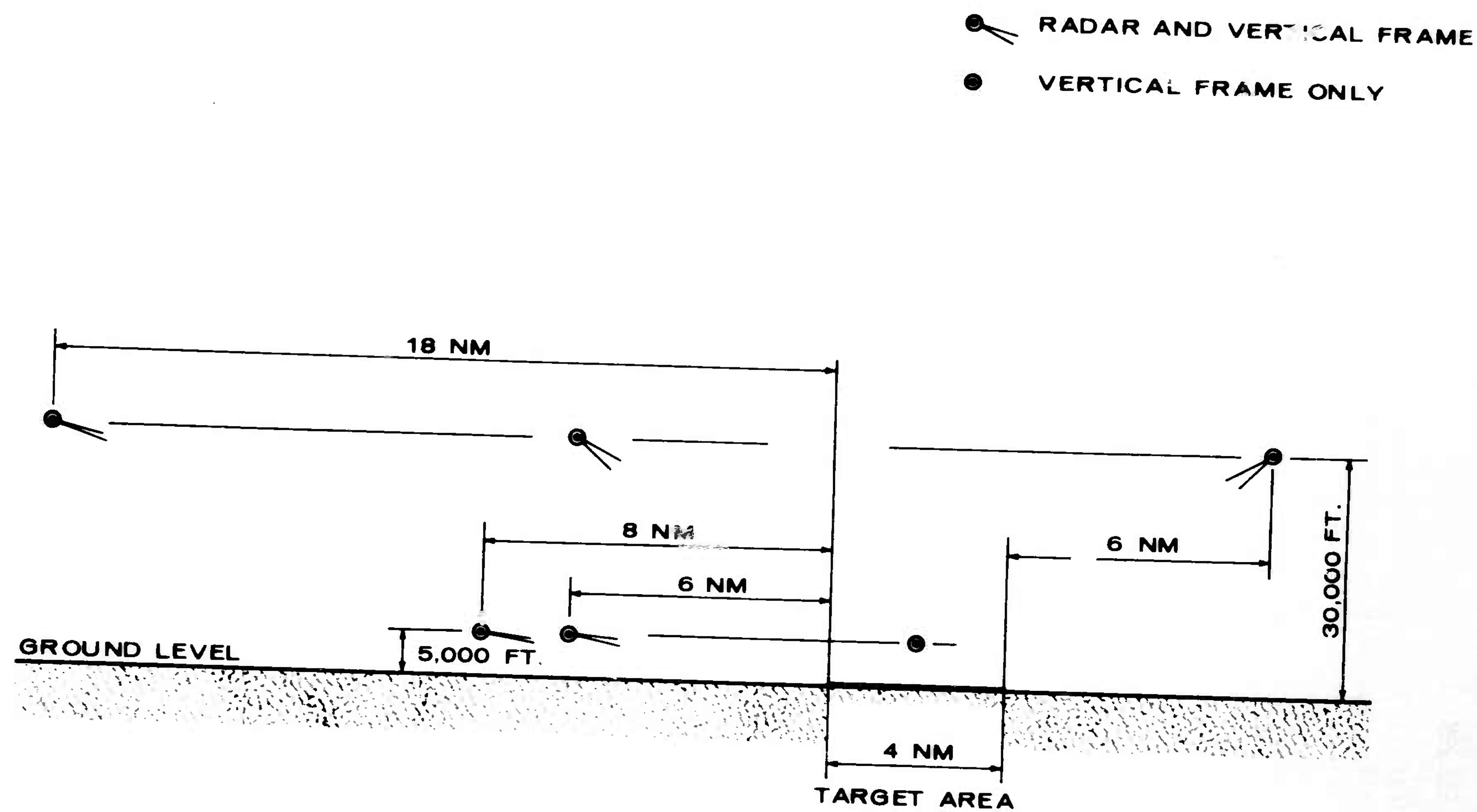

FIGURE 1. STEREO FLIGHT CONFIGURATION, AS PLANNED

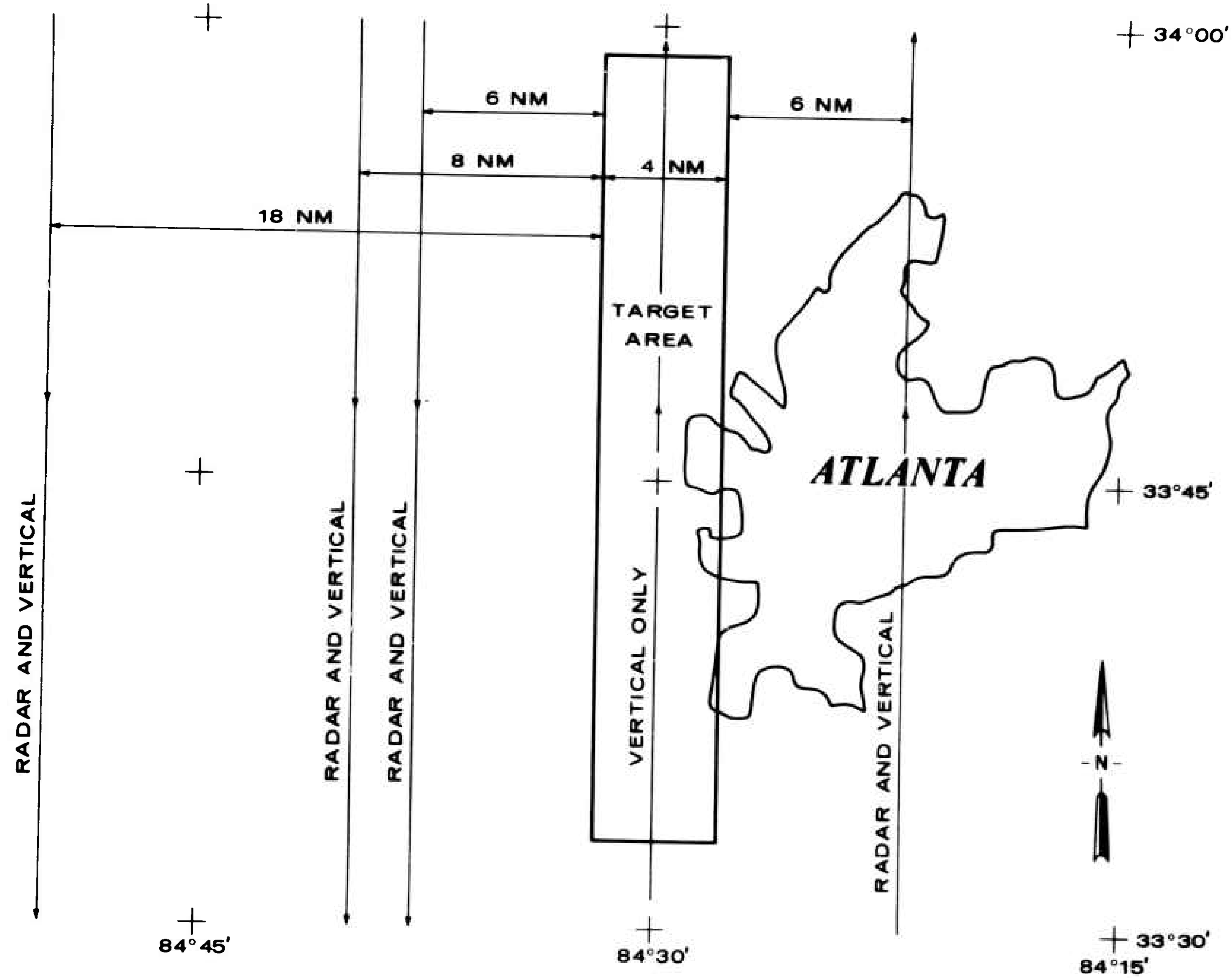

FIGURE 2. FLIGHT PLAN

Generally speaking, the flights followed the flight design given in Figures 1 and 2 fairly well. The only significant departure from the plan related to the photography-only flight made directly over the target area. This pass was flown at high altitude, rather than at low altitude as originally planned, probably to ensure adequate lateral coverage of the target area with the KC-1B camera.

1.4 Scope of the Investigation

This investigation is essentially a test of the mapping accuracy of the AN/APQ-102(XA-2) side-looking radar, using real data taken under real flight conditions over a prescribed target area. The test not only includes evaluation of planimetric accuracy but also élevation accuracy as well under stereo radar conditions. The two basic stereo radar configurations (opposite-side and same-side cases) are considered.

An essential prerequisite for the test is development of a suitable procedure tailored to handle the test material actually acquired. Development of the test procedure, along with performance of the test itself, is included within the scope of the investigation.

The project is divided into the following ten tasks:

Task 1: Inspection, Evaluation and Selection of Test Material.
Task 2: Design of Test Procedure.
Task 3: Mathematical Analysis and Programming.
Task 4: Radar Mensuration.
Task 5: Aerotriangulation of Photography Flown Simultaneously With Radar.
Task 6: Aerotriangulation of Photography of the Test Area.
Task 7: Radar Data Processing.
Task 8: Analysis of Results.
Task 9: Preparation of Interim Technical Report.
Task 10: Preparation of Final Technical Report.

Tasks 1, 2 and 3 are directed toward development of a suitable test procedure. Task 1 assesses the quantity, quality and completeness of the material provided for the test, and selects a specific test area; Task 2 designs the test procedure on the basis of information found in Task 1; and Task 3 implements the design by developing the necessary software.

Tasks 4 through 8 perform the test. Tasks 4 through 7 are accomplished in accordance with the test procedure developed in Tasks 1, 2 and 3; and Task 8 analyzes the test results.

Tasks 9 and 10 document the work. The Interim Technical Report was prepared in February 1970, following some initial test results. The Final Technical Report, this report, documents the entire investigation, including the work described in the Interim Technical Report.

2. INVESTIGATION

2.1 Inspection, Evaluation and Selection of Test Material (Task 1)

This task was necessarily the first to be accomplished, since design of the test procedure was heavily dependent upon the quality, quantity and completeness of data provided. Upon receipt of the radar imagery, vertical photography and other supporting information, the records were inspected closely and organized as to content to aid in the selection of specific material for the investigation.

Initial inspection of the data directed attention to several problem areas which might at least hinder, if not directly affect, the results of the investigation. Specifically, for the KC-1B vertical frame photography taken simultaneously with radar coverage of Sortie 08-61:

a) The film was badly fogged, apparently in the developing stage, to the extent that much resolution was lost, totally in some areas.

b) No camera calibration data were supplied for the camera used (KC-1B-Lens Cone No. 316). As a result, no compensation could be made for film distortion, and a fictitious set of master fiducial coordinates would have to be deduced from comparator measurements in order to make possible the transformation from comparator readings to plate coordinates.

c) Only three fiducial marks were imaged on each frame, and, of the three, one was a partial image of irregular shape.

d) Cloud cover was considerably higher than the normally accepted limit.

e) Trees were in complete foliage, creating difficulties in point selection and identification.

f) Frame spacing was irregular, ranging from about 400 meters to over 6000 meters (Approximately 95% endlap to 60% endlap).

g) The frame clock was not running.

Radar imagery was judged to vary from good to poor, having inconsistent resolution from one strip to another. Most resolution problems were associated with image streaking, image fading, or overall poor contrast. The absence of time marks and range marks on the radar imagery indicated special problems which would have to be dealt with in the design of the test procedure.

A specific objective of Task 1 was selection of a test area and corresponding radar and frame camera imagery to be used in the investigation. The flight plan (Figures 1 and 2) presented several possibilities in forming radar stereomodels of the test area. All possible configurations were examined, and one radar stereomodel was chosen for each of the two general cases (opposite-side and same-side) of stereo radar geometry.

The opposite-side case chosen (See Figure 3) consists of two passes offset six nautical miles to either side of the target area, both at an altitude of approximately 32,000 feet AGL (Actual flight altitude was higher than planned). This configuration is geometrically the strongest available, giving range intersection angles of about 105° throughout the target area. The two flights comprising the same-side case are offset six and eighteen nautical miles to one side of the target area (Figure 3), both at an altitude of approximately 32,000 feet AGL (again, slightly higher than planned). This combination was thought to offer the best visual stereomodel of those available. The low altitude radar imagery was dropped from consideration because of its poor quality.

The opposite-side case was designated Stereo Radar Model I; the same-side case, Stereo Radar Model II. The specific test area selected is a rectangular strip, approximately 5 miles long by 3 miles wide, shown in Figure 4. The specific radar records which were selected are:

(1) Sortie 08-61, Pass 3, Channel A.
(2) Sortie 08-61, Pass 4, Channel B.
(3) Sortie 08-61, Pass 5, Channel A.

For sake of brevity, these records will be referred to simply as Passes 3, 4 or 5, or as Strips 3, 4 or 5. They are shown in Figure 3.

Passes 3 and 4 make up Stereo Radar Model I (opposite-side case); Passes 3 and 5 make up Stereo Radar Model II (same-side case).

The original plan anticipated using the entire target area for the test. However, in view of the inconsistent quality of photography and radar imagery, it was decided to confine the test to a small area where the radar image quality, at least, was as good as possible.

The displacement of the centerline of the test area with respect to the target area, very apparent in Figure 4, is caused by using only one channel of each pass. Both channels. side by side, cover a swath somewhat wider than the target area.

KC-1B vertical frame photography, taken simultaneously with the selected radar passes, was indexed to USGS Topographic Maps. In addition, a two-frame model of vertical photography covering the test area was identified and selected from Sortie 08-212. The KS-72 frame photography did not have to be used.

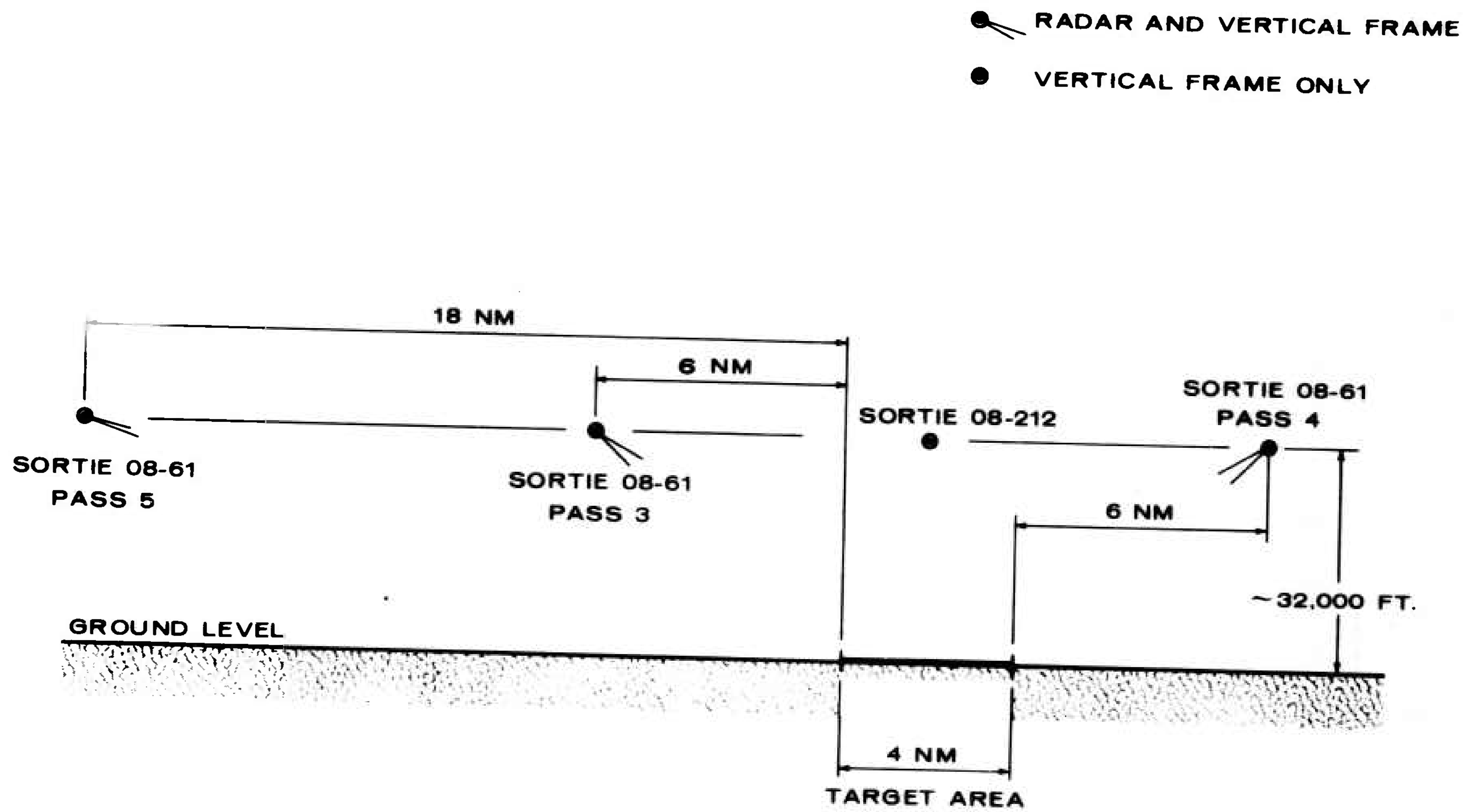

FIGURE 3. STEREO FLIGHT CONFIGURATIONS ACTUALLY USED IN THE TEST

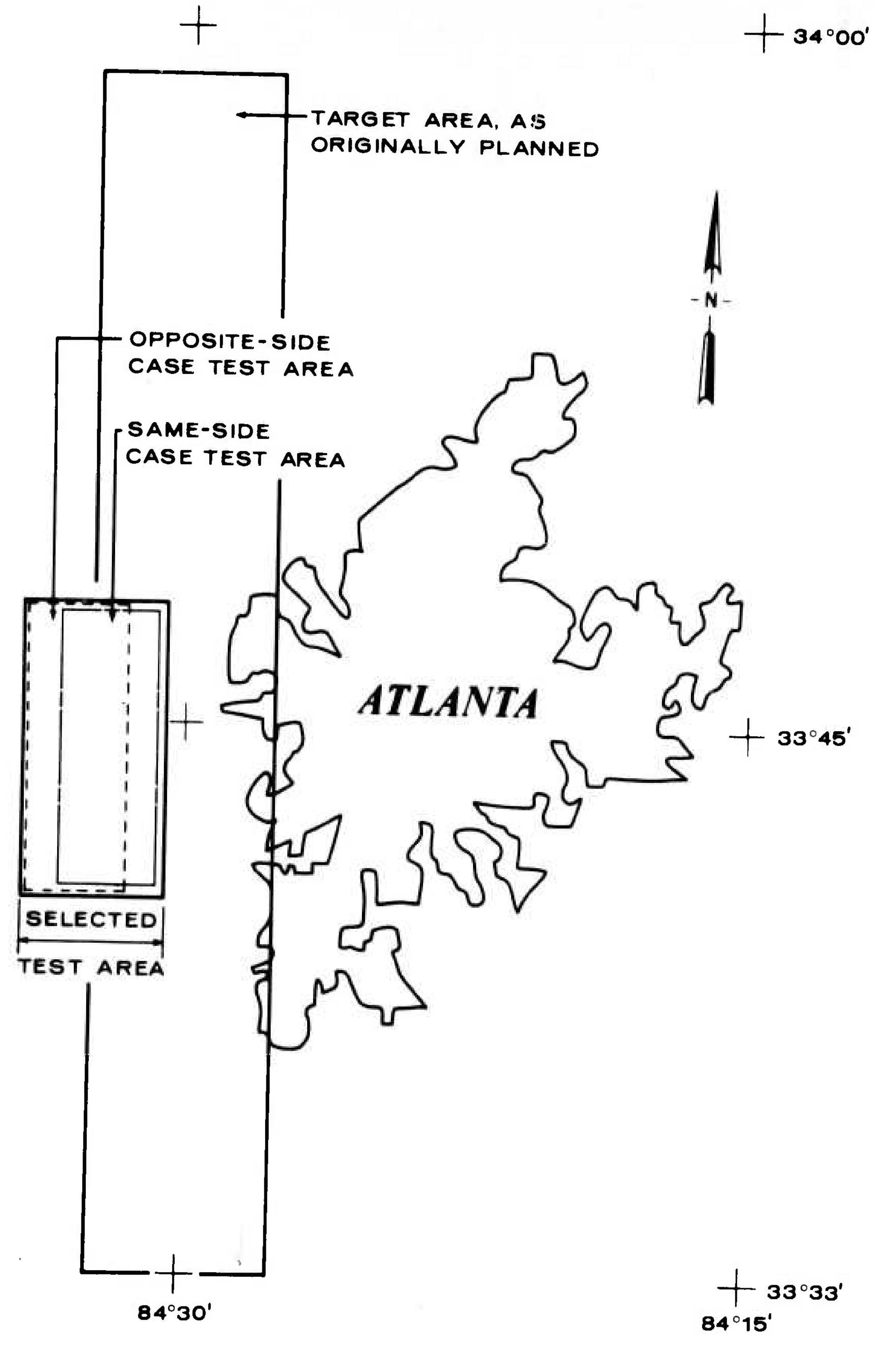

FIGURE 4. SELECTED TEST AREA

2.2 Design of Test Procedure (Task 2)

The original test approach presumed that each radar record would have range marks in the across-flight direction and time marks in the along-flight direction to permit direct recovery of slant range and time from the record with minimal error. Furthermore, it was assumed that precise times of exposure of the cartographic camera, operating simultaneously with the radar, would be suitably indexed on the corresponding radar record to permit direct correlation between photography and radar imagery. Data reduction could then proceed in an orderly manner; that is, the camera air station positions could first be determined, then the radar air stations could be interpolated from the camera stations with aid of the recorded time marks, then the slant ranges could be extracted directly from the radar record, and finally, the ground positions of the test points could be intersected.

Since the actual radar imagery which was received had neither range marks, nor time marks, nor any index marks to correlate the cartographic camera exposures to the radar imagery, an approach different from that just described had to be adopted. Specifically, it was necessary to introduce an artificial time scale and make use of ground control located in the test area. The ground control points have known ground positions, and are also imaged on the radar records. This provides a tie between the radar records and the ground, in much the same way that ground control ties aerial photography to the ground in an aerotriangulation.

Information derived from the ground control can be used to locate the radar air stations along the flight path and to calibrate the radar range measurements. In this particular approach, the camera air stations serve only to define the flight path, independent of time. In other words, without any correlation between camera exposures and radar record, radar air stations cannot be time-interpolated between the camera stations; instead, the ground control is used to locate specific radar air stations along the flight path, from which the remaining radar air stations are interpolated.

Once radar air station positions and slant ranges have been found, intersection of the test points proceeds as in the original approach.

The specific steps taken are now outlined:

1. Lay off a reference line at the side of each radar image strip (Figure 5). This line can be defined by two finely marked holes (reference points) in the emulsion. The reference line serves as the t-axis of the radar image; the r-axis is defined to be perpendicular to the t-axis and to pass through the first reference point.

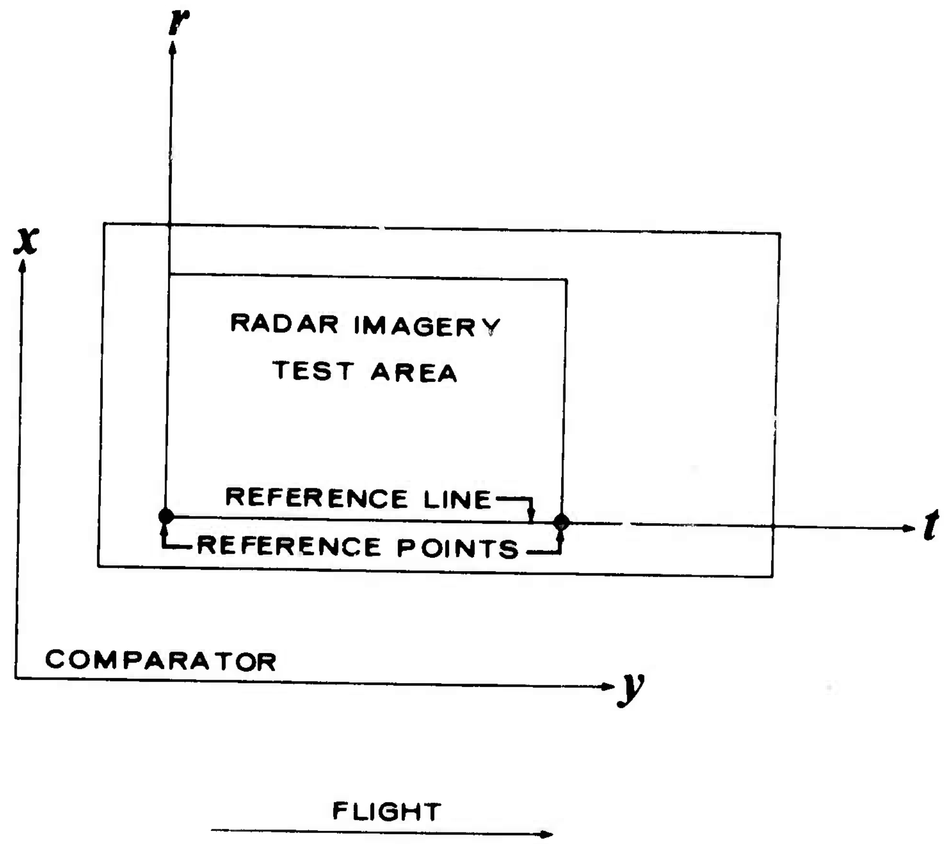

FIGURE 5. MENSURATION OF RADAR IMAGERY

2. Select and mark a number of points which are identifiable in each radar image strip and in the test area photography. Select several of these points as control points; the remaining points are used as test points.

3. On each radar image strip, measure the (x,y) coordinates of all points (control points, test points, and the points defining the reference line) with a high-precision comparator.

4. Transform the image coordinates of all points to the (r,t) plate coordinate system. The r-coordinates are uncalibrated measures of slant range; the t-coordinates serve as artificial measures of time.

5. Aerotriangulate the photography flown simultaneously with the radar to obtain the camera station positions in space.

6. Aerotriangulate the test area photography to establish the ground positions of the control points and test points within the test area.

7. Interpolate the triangulated camera station positions to obtain the flight path in space for each radar pass.

8. Locate the zero-Doppler line for each control point. Then locate the position of the radar air station on the flight path at the base of the zero-Doppler line. (Note: for a specific point on the ground, the zero-Doppler line is perpendicular to the flight path and passes through the point, as shown in Figure 6. The radar air station is considered to be located where the radar actually was in space at the moment it was looking at the point along the zero-Doppler line).

9. Determine the slant range for each control point, using the known ground and radar air station coordinates. At this point, in addition to the given ground coordinates, the following data are known for each control point:

   (a) Radar air station position.
   (b) Slant range.
   (c) The t-coordinate ("time"), and the r-coordinate.

10. Calibrate the r-coordinates of the control points against their known slant ranges. The calibration curves, one for each flight, can be represented

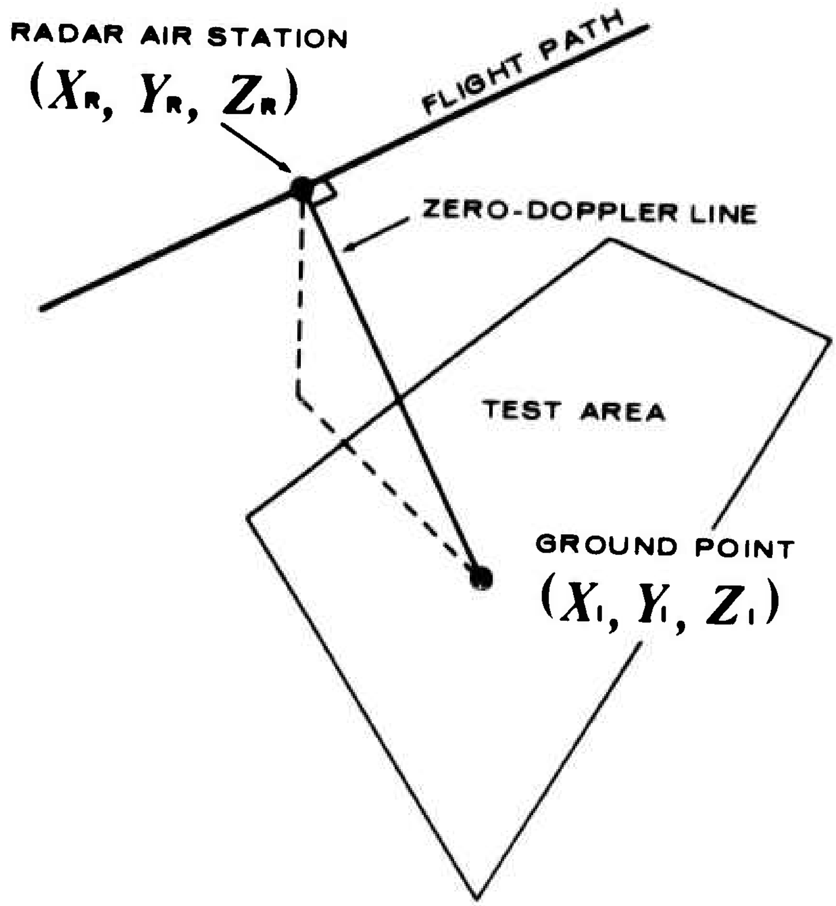

FIGURE 6. ZERO-DOPPLER CONDITION

graphically, or analytically by a polynomial function. This, in effect, substitutes for the range marks.

11. Construct for each flight an ephemeris of radar air station positions in terms of the artificial time scale.

12. Using the slant range calibration curves, determine the slant ranges for all test points from their r-coordinates.

13. Interpolate the radar air station position for each test point, using the t-coordinate of the test point and the ephemeris constructed in Step 11.

14. Intersect the position of each test point, using the computed radar station positions and slant ranges from each of the two flights comprising the stereo configuration. Note that Steps 1 through 13 deal with each flight separately. Step 14 finally merges together the data from both flights.

15. Compare the intersected positions of the test points with their positions established by aerotriangulation in Step 6.

Steps 1 through 4 are the essential ingredients of Task 4 (Radar Mensuration). Step 5 corresponds with Task 5 (Aerotriangulation of Photography Flown Simultaneously with Radar), and Step 6 corresponds with Task 6 (Aerotriangulation of Photography of Test Area). Steps 7 through 14 are performed in Task 7 (Radar Data Processing), and Step 15 is included in Task 8 (Analysis of Results).

2.3 Mathematical Analysis and Programming (Task 3)

The salient features of the mathematical analysis and programming for Task 7 (Radar Data Processing) are presented in this section. More detailed mathematical formulation is given in the Appendix of this report.

Section 2.3.1, which follows, is essentially Step 7 of the Test Procedure; Section 2.3.2 combines Steps 8 and 9; Section 2.3.3 is Step 10; Section 2.3.4 is Step 11; and Section 2.3.5 combines Steps 12, 13 and 14.

2.3.1 Interpolation of Flight Path

Camera station positions along the flight path can be established by photogrammetric aerotriangulation. Other points on the flight path can then be located by interpolation between successive camera stations. The camera station positions and interpolation functions thus define the flight path in space.

Inspection of the particular test material to be used in this study already revealed considerable irregularity in camera station spacing (see Section 2.1, Item (f)), with some intervals between successive camera stations extending more than 6000 meters (Figure 11, appearing later in Section 2.5, shows the irregular camera station spacing). It was felt that the excessive separation between camera stations did not justify use of anything other than linear interpolation between successive stations. Thus, the flight path was defined by a set of line segments connecting successive camera stations.

2.3.2 Determination of Radar Air Station Position and Slant Range for Each Control Point

It is assumed that the cartographic camera and radar antenna are located at essentially the same position in the aircraft; that is, there is negligible physical displacement between the camera and antenna center. Hence, the flight path defined by the camera stations is also assumed to be the flight path of the radar.

Once the radar flight path has been defined, the radar air station for each control point can be located. This is done by constructing the control point's zero-Doppler line; that is, a line perpendicular to the flight path and passing through the control point (Figure 6). The base of the perpendicular locates the position of the radar, the radar air station, at the time the control point was imaged on the radar record. (Actually, the radar imaging process for a coherent system is more involved than what this simple geometrical model indicates in that the radar is really collecting an extended phase history of the control point as the aircraft travels over a sizeable portion of the flight path. However, subsequent construction of the radar image in a correlator-processor is done in such a way that the control point can be taken as viewed simply along the zero-Doppler line.)

The radar air station position (X_R, Y_R, Z_R) is obtained by solving the following three equations:

$$\alpha(X_R - X_I) + \beta(Y_R - Y_I) + \gamma(Z_R - Z_I) = 0 \quad (1)$$

$$X_R = X_o + \frac{\alpha}{\beta}(Y_R - Y_o) \quad (2)$$

$$Z_R = Z_o + \frac{\gamma}{\beta}(Y_R - Y_o) \quad (3)$$

in which α, β and γ are the direction numbers of the flight path segment in which the radar air station lies; X_o, Y_o and Z_o are the coordinates of the camera station which initiates the flight path segment; and X_I, Y_I and Z_I are the ground coordinates of the control point.

If the zero-Doppler line is taken normal to the ground track of the flight path, rather than to the flight path itself, the third term of Equation (1) is eliminated first before solving for the radar air station position. For a nearly level flight path, there should be little difference between using the flight path or ground track, because for this situation γ is already very small.

Once the position of the radar air station is known, the slant range (SR_I) to the control point can be computed:

$$SR_I = [(X_R - X_I)^2 + (Y_R - Y_I)^2 + (Z_R - Z_I)^2]^{\frac{1}{2}} \qquad (4) .$$

Slant ranges computed for several control points will be used to determine the slant range calibration function.

2.3.3 Slant Range Calibration

It is assumed that a preliminary transformation (Step 4 of the test procedure outlined in Section 2.2) has first been made to put all image coordinates measured in the comparator (x,y) coordinate system into the plate (r,t) coordinate system defined by the reference points (Figure 5). If the reference points have been carefully chosen, the r-coordinate will be essentially an uncalibrated measure of slant range. However, to account for any error in the direction of the selected reference line, a new coordinate system (R,T) is introduced, Figure 7, in which the T-axis makes a small angle θ with the t-axis. All points on the T-axis are presumed to have the same slant range, and the R-coordinates can then be directly related to slant range. Finding θ, of course, is an added requirement.

The plate coordinates, R_I and T_I, of the image of point I are related to the plate coordinates r_I and t_I by the following equations:

$$R_I = r_I \cos \theta + t_I \sin \theta \qquad (5)$$

$$T_I = t_I \cos \theta - r_I \sin \theta \qquad (6) .$$

Now the slant range, SR_I, for point I is assumed to be a second-order polynomial function of the R_I-coordinate; that is,

$$SR_I = A_{SR} + B_{SR} R_I + C_{SR} R_I^2 \qquad (7) .$$

This is an empirical relationship, but, nevertheless, a realistic one. The constant term, A_{SR}, is the slant range for points whose images lie right on the T-axis; the coefficient B_{SR} is a scale factor, relating distances measured along the R-axis to corresponding slant ranges; and the coefficient C_{SR} accounts for any linear variation, hopefully small, in the scale across the radar record.

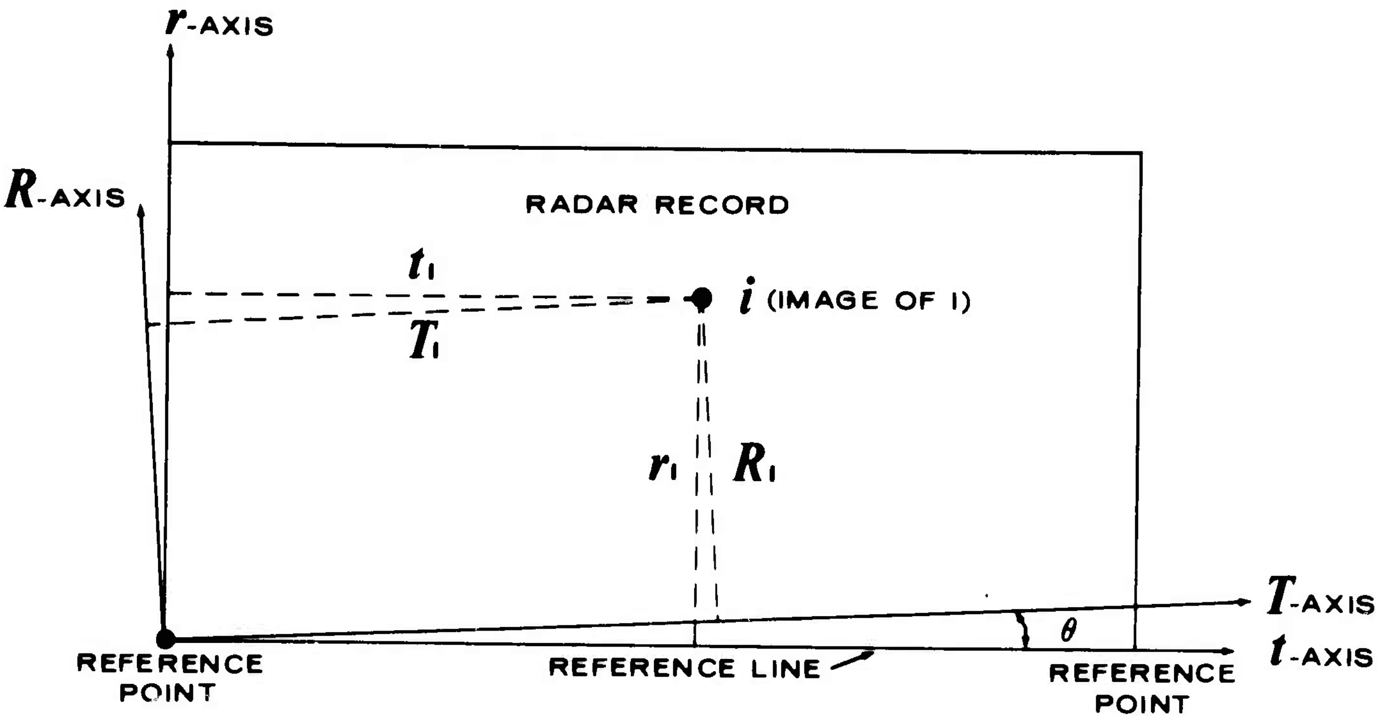

FIGURE 7. PLATE COORDINATE SYSTEMS FOR RADAR IMAGERY

Slant range calibration can be accomplished by fitting the polynomial (Equation (7)) to data obtained for control points imaged in the radar record. The fit is best made using the method of least squares, which, in addition to the polynomial coefficients A_{SR}, B_{SR} and C_{SR}, also solves for the unknown rotation angle, θ. The form of the condition equations used in the least squares solution is obtained by substituting the right-hand side of Equation (5) for R_I in Equation (7); thus,

$$SR_I = A_{SR} + B_{SR}(r_I \cos\theta + t_I \sin\theta) + C_{SR}(r_I \cos\theta + t_I \sin\theta)^2 \qquad (8) .$$

Once the parameters (A_{SR}, B_{SR}, C_{SR} and θ) of the calibration have been determined for a particular radar record, slant ranges for all other points imaged and measured (known r_I and t_I) in the record can be obtained using Equation 8. In particular, the slant ranges for the test points can be computed. However, this computation is not actually made at this time. Instead, it is incorporated into the least squares intersection computation which follows later.

If the radar exhibits stability in the display of slant range (i.e., the coefficients B_{SR} and C_{SR} remain almost constant from one record to the next), information from two or more records can be combined to determine common values for B_{SR} and C_{SR}. The other parameters, A_{SR} and θ, must still be evaluated for each individual record, however, since they depend upon selection of the reference points, which is somewhat arbitrary.

2.3.4 "Time" Correlation

A necessary step in the data reduction is correlation of the radar air station positions with the radar record. More specifically, functions must be obtained which can be used to determine the radar air station positions from measured image coordinates on the radar record. Radar air station positions have already been determined for the control points. Furthermore, these points have been identified and measured on the radar record. Thus, a positive relationship between the radar record and the radar air stations can be established through the ground control.

The T-axis defined in Section 2.3.3 can be regarded as an "improved" time axis, in the sense that it is an improvement over the t-axis defined by the arbitrarily selected reference points. The T-coordinates are still artificial measures of time, though, since no real time was actually recorded during operation of the radar. However, it is really immaterial whether the T-coordinates are real or artificial measures of time, since all that is needed is an independent variable for interpolation of the radar air stations. Conveniently, the plate coordinate, T_I, is selected as the independent variable, and interpolation of radar air station coordinates can be done using the following "time" polynomials:

$$X_{R_I} = A_X + B_X T_I + C_X T_I^2 + \ldots \tag{9}$$

$$Y_{R_I} = A_Y + B_Y T_I + C_Y T_I^2 + \ldots \tag{10}$$

$$Z_{R_I} = A_Z + B_Z T_I + C_Z T_I^2 + \ldots \tag{11}$$

in which X_{R_I}, Y_{R_I}, Z_{R_I} are the coordinates of the radar air station for the Ith ground point; and A_X, B_X, C_X, A_Y, B_Y, C_Y, A_Z, B_Z, C_Z, etc., are polynomial coefficients which have to be first evaluated.

Evaluation of the polynomial coefficients can be accomplished by fitting the time polynomials to known data (X_{R_I}, Y_{R_I}, Z_{R_I} and T_I) for the control points. A separate set of coefficients is found for each flight segment, using the method of least squares. Because each flight segment is a straight line, the A-coefficients are necessarily related in accordance with Equations (2) and (3), as are the B-coefficients, C-coefficients, and so on. Furthermore, if the ratio of aircraft ground speed to radar data film speed is constant, second and higher order terms in the "time" polynomials are zero, and the interpolation of radar air stations along the flight path is linear with respect to T_I.

Once the polynomial coefficients have been found for each flight line segment, the radar air station position for any test point can be computed using the time coordinate, T_I, of the point's image on the radar record. However, as with the point's slant range, this computation is not actually made at this time, but is incorporated into the least squares intersection computation which follows.

2.3.5 Intersection Geometry

If, for any given test point, the direction of flight, slant range and radar air station position are known, or readily determinable, for each of two radar flights making up a stereo radar model, the position of the test point can be intersected in space. Computation of all data necessary for the space intersection has already been dealt with in Sections 2.3.1 through 2.3.4, and so these data are now presumed to be available.

For any test point, I, imaged in the two radar records making up the stereo radar model, four equations can be written expressing slant range and zero-Doppler conditions for the point's intersection. Specifically, for the first radar record:

$$[(X_I - X_{R_1})^2 + (Y_I - Y_{R_1})^2 + (Z_I - Z_{R_1})^2]^{\frac{1}{2}} = SR_{I_1} \quad (12)$$

$$\alpha_1(X_I - X_{R_1}) + \beta_1(Y_I - Y_{R_1}) + \gamma_1(Z_I - Z_{R_1}) = 0 \quad (13) ,$$

and for the second radar record:

$$[(X_I - X_{R_2})^2 + (Y_I - Y_{R_2})^2 + (Z_I - Z_{R_2})^2]^{\frac{1}{2}} = SR_{I_2} \quad (14)$$

$$\alpha_2(X_I - X_{R_2}) + \beta_2(Y_I - Y_{R_2}) + \gamma_2(Z_I - Z_{R_2}) = 0 \quad (15) .$$

In these equations, X_{R_1} , Y_{R_1} and Z_{R_1} are the coordinates of the first radar air station (pertaining to the first radar record), and X_{R_2} , Y_{R_2} and Z_{R_2} are the coordinates of the second radar air station; α_1 , β_1 and γ_1 are the direction numbers of the first flight path (pertaining to the first radar record), and α_2 , β_2 and γ_2 are the direction numbers of the second flight path; SR_{I_1} is the slant range to I from the first radar air station, and SR_{I_2} is the slant range to I from the second radar air station; and X_I, Y_I and Z_I are the unknown ground coordinates of I.

Equations (12) and (14) express the slant ranges between radar air station R_1 and test point I, and radar air station R_2 and I, respectively, in terms of the object space coordinates of the points. Equations (13) and (15) express the orthogonality of the flight paths and the corresponding zero-Doppler lines in terms of direction numbers.

Since four equations are used to solve for the three unknown coordinates (X_I, Y_I, Z_I), a least squares solution is employed. In this solution, the plate coordinates, R_I and T_I, implicit in the slant range and in the radar air station coordinates, are taken as the observations. Equations (7), (9), (10) and (11) are thus included with Equations (12) through (15) to form the condition equations of the least squares solution. By setting up the condition equations in this manner, prior computation of slant range and radar air station coordinates is not required.

It might be noted at this point that two positions of intersection can be obtained for each test point, since each pair of equations ((12)/(13) and (14)/(15)) defines a circle in space, and the two circles thus defined by all four equations can intersect at two points. In practice, this ambiguity presents no problem so long as reasonably good estimates of X_I, Y_I and Z_I are given in the first place to initiate the least squares solution.

2.3.6 Error Propagation

A useful feature of the least squares solution is provision of a model for propagating errors in the observed quantities into the final results. The error propagation model is derived directly from the inverse of the coefficient matrix of the normal equations constructed during the course of the least squares solution. In the case at hand, measures of precision for the computed ground coordinates, X_I, Y_I, Z_I, can be obtained from the least squares intersection, based upon precisions of the image coordinates, R_I and T_I.

The measures of precision for X_I, Y_I and Z_I are necessarily dependent upon the precisions assigned R_I and T_I. Hence, the assigned precisions should be as realistic as possible to make any sense out of the results.

The least squares intersection solution assumes that the slant range calibration constants and other determined coefficients included in the condition equations are errorless, which is not entirely correct. Nevertheless, in spite of this shortcoming, the error propagation is still able to give insight into the precision with which test point positions can be determined using this particular stereo radar technique.

2.3.7 Computer Programs

Four computer programs were prepared to accomplish the radar data reduction. Brief descriptions of these programs are given:

Program 1: This computer program defines the flight path, and determines the radar air station positions for the known control points using the zero-Doppler condition. It also computes the slant ranges for the control points. The mathematical analysis for the program is described in Sections 2.3.1 and 2.3.2. The program has the option of defining the zero-Doppler line normal to the flight path or normal to the ground track.

Program 2: This is the slant range calibration program. In accordance with the mathematical analysis given in Section 2.3.3, this program uses the method of least squares to find the slant range calibration parameters. The program allows for processing all radar records separately or together. Computation of slant range residuals is included.

Program 3: This program performs the "time" correlation described in Section 2.3.4. Specifically, it computes least squares estimates of the time polynomial coefficients from control point data.

Program 4: This is the intersection program. In accordance with the analysis outlined in Section 2.3.5, this program computes,

by intersection, the positions of the test points on the ground. The program has the option of defining the zero-Doppler line normal to the flight path or normal to the ground track. A least squares solution, including error propagation (Section 2.3.6), is used.

All programs were written in FORTRAN IV for the IBM 360/44 computer.

2.4 Radar Mensuration (Task 4)

The sections of radar Strips 3, 4 and 5 of Sortie 08-61, making up the two models under consideration (Model I, opposite-side case, Strips 3 and 4; Model II, same-side case, Strips 3 and 5), were contact printed onto glass diapositive plates. Under optical magnification, a number of points (to be used as control and test points) were carefully selected and marked on each plate for measurement on the Mann comparator. All points selected were also identifiable on the aerial photography of the test area. A total of 60 points were selected on Strip 3, 55 on Strip 4, and 30 on Strip 5. Fewer points were selected on Strip 5 because there was less detail appearing on that strip. Of the points selected, 49 were common to Strips 3 and 4, and so could be used for Model I (Figure 8). All 30 points selected on Strip 5 also appeared on Strip 3, and so could be used for Model II (Figure 9). Twenty-five points were common to both radar models.

Each image selected for measurement was marked on the Wild PUG point transfer device by drilling a 50-micrometer (μm) hole in the plate emulsion. Radar Strips 3 and 5 (Model II, same-side case) were viewed stereoscopically, and 22 of the 30 points selected on Strip 5 were drilled on that strip in this mode. Extensive efforts were made to view and mark points stereoscopically in the opposite-side case (Model I), with unsatisfactory results. Consequently, the points on Strips 3 and 4 were marked monoscopically.

A reference line was established on each radar record by drilling two 50-micrometer (μm) holes in the plate emulsion at each end of the test area, along the near edge of the imagery. This reference line, constructed as nearly parallel to the edge of the imagery as visual means allowed, forms the basis of the radar plate coordinate system into which the comparator measurements are transformed (Figure 5). The along-flight direction (the reference line itself) defines the artificial time scale by which image points can be correlated with radar air station positions. The axis normal to the time axis is taken as the range scale.

Coordinates (x,y) of all radar image points and reference points were carefully measured on the glass diapositive plates with the Mann comparator. The measurements were then transformed to the plate coordinate system (r,t) defined by the reference points.

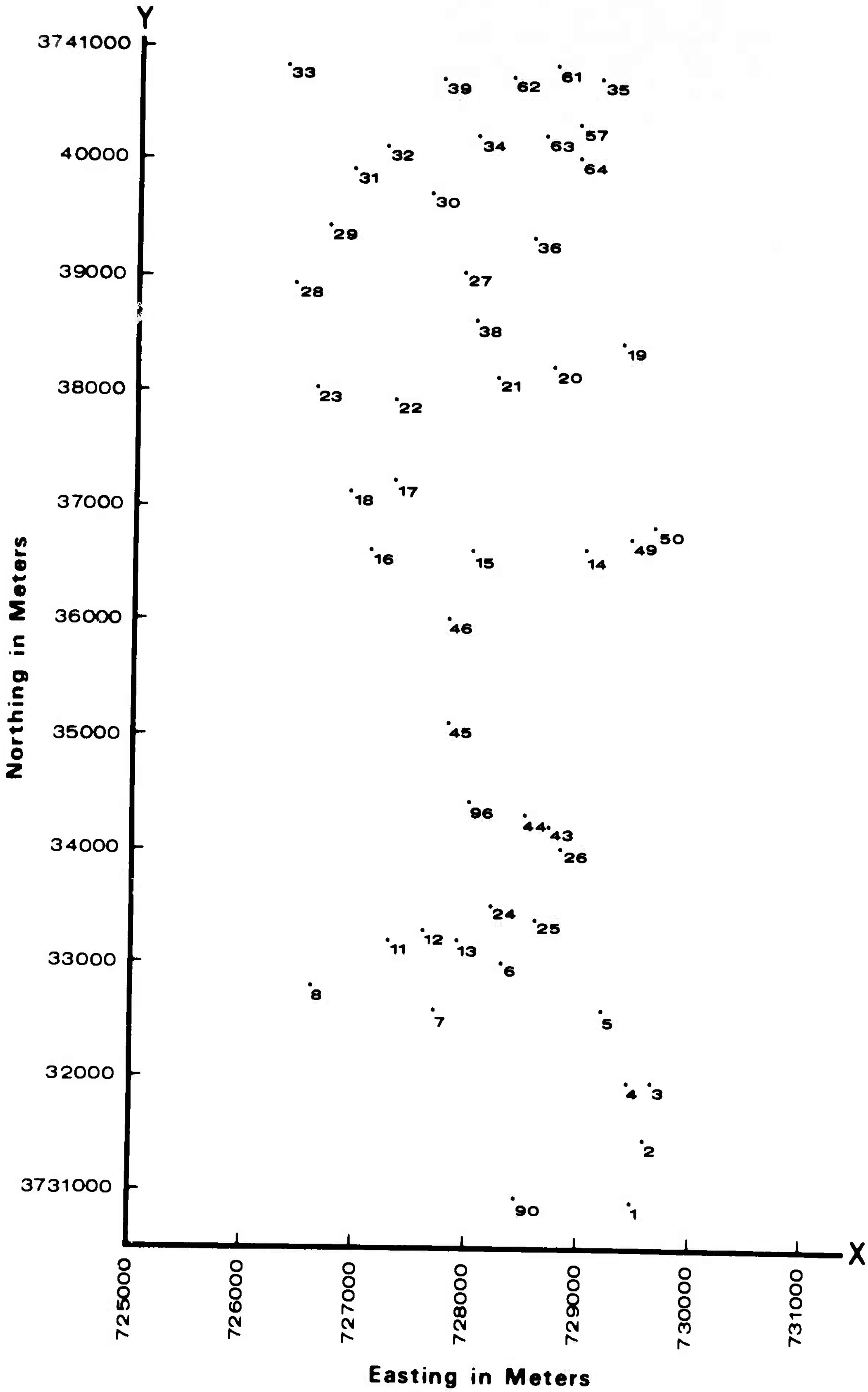

FIGURE 8. SELECTED GROUND POINTS-MODEL I (OPPOSITE-SIDE CASE)

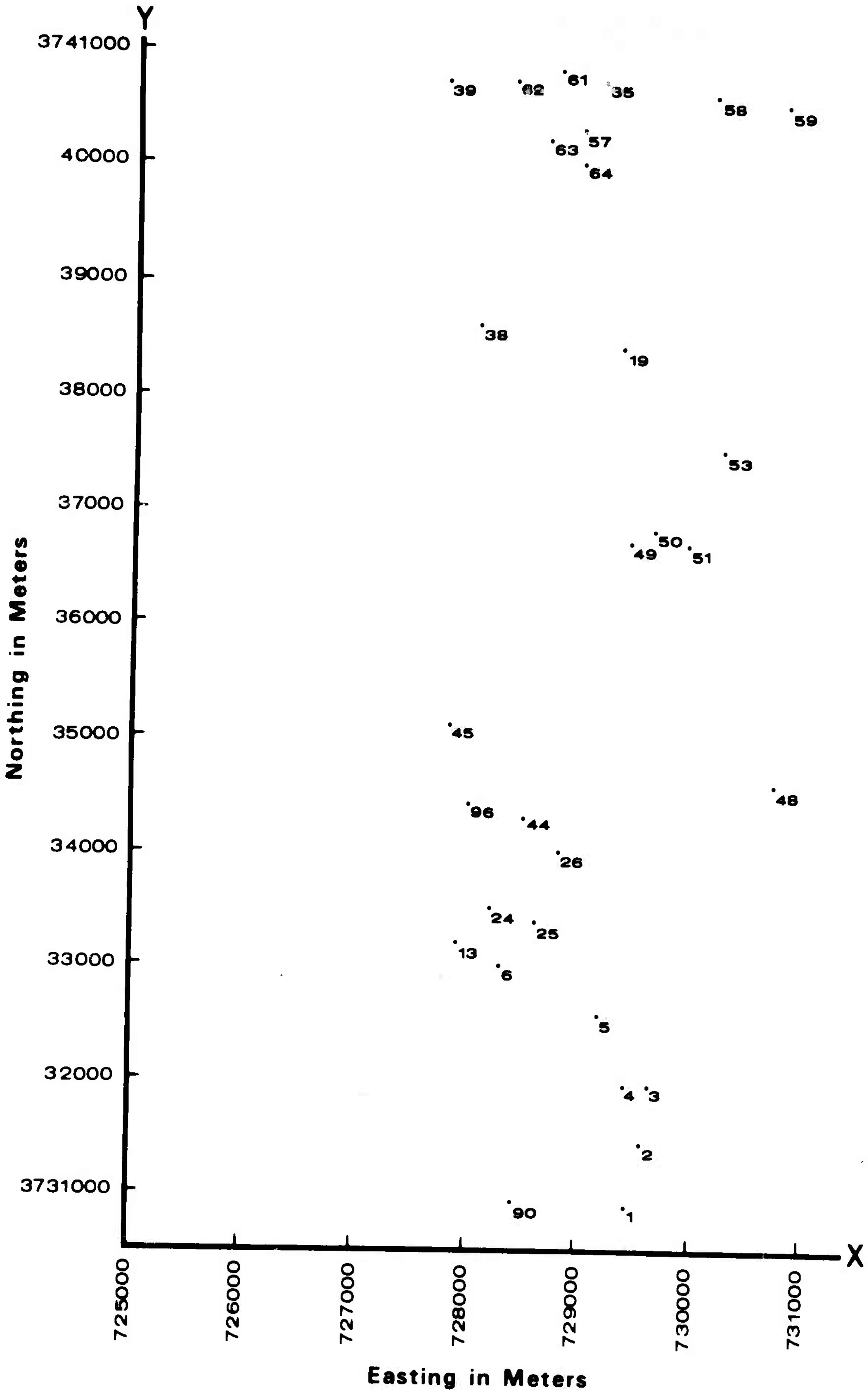

FIGURE 9. SELECTED GROUND POINTS–MODEL II (SAME-SIDE CASE)

2.5 Aerotriangulation of Photography Flown Simultaneously With the Radar (Task 5)

Vertical photography, flown simultaneously with the radar coverage of the test area, was photogrammetrically aerotriangulated to establish the flight path of the aircraft (and of the radar) at the time of flying the radar. Camera station coordinates were determined for each frame of photography in the three strips selected for the study (Strips 3, 4 and 5 of Sortie 08-61), giving for each strip a set of discrete points along its flight path.

Ten frames in Strip 3, 9 frames in Strip 4, and 14 frames in Strip 5 were selected for aerotriangulation. The frames were contact printed onto film positives, and several points (9-21 per frame) were selected for mensuration and marked. Mensuration was then accomplished on a Mann precision comparator.

Preprocessing of image coordinates for the aerotriangulation had to be tailored to accommodate the available camera data, incomplete as it was. No compensation could be made for film distortion, and a set of master fiducial mark coordinates had to be artifically deduced from comparator measurements of the three available fiducial marks in order to define the position of the principal point (Figure 10).

A lens distortion table for the camera (KC-1B, Lens Cone No. 316) was extracted from U.S. Army Geodesy, Intelligence and Mapping Research and Development Agency Technical Note 66-2, "The Calibration of Military Cartographic Cameras", and applied in the preprocessing of plate measurements. The corresponding calibrated focal length was also obtained from the same source. In addition, plate coordinates were corrected for effects of atmospheric refraction.

Ground control used for the aerotriangulation of Strips 3 and 4 was scaled from 1:24,000 USGS quadrangle maps (UTM grid), and that for Strip 5 was scaled from USGS maps at 1:62,500 scale. Standard deviations of 12 meters in X and Y and 2 meters in elevation were assigned to the control for weighting purposes.

The strips were aerotriangulated using a well-established analytical least squares solution. Data reduction, including error propagation, was performed using Autometric's in-house IBM 360/44 computer. The a posteriori variance of unit weight computed from the least squares solution indicated a standard deviation of 0.040 mm in the measurement of each image coordinate. This seems to be a reasonable value, considering the quality of the photography and the incomplete camera calibration data.

The aerotriangulation is briefly summarized in Table I. The triangulated camera station positions are plotted in Figure 11.

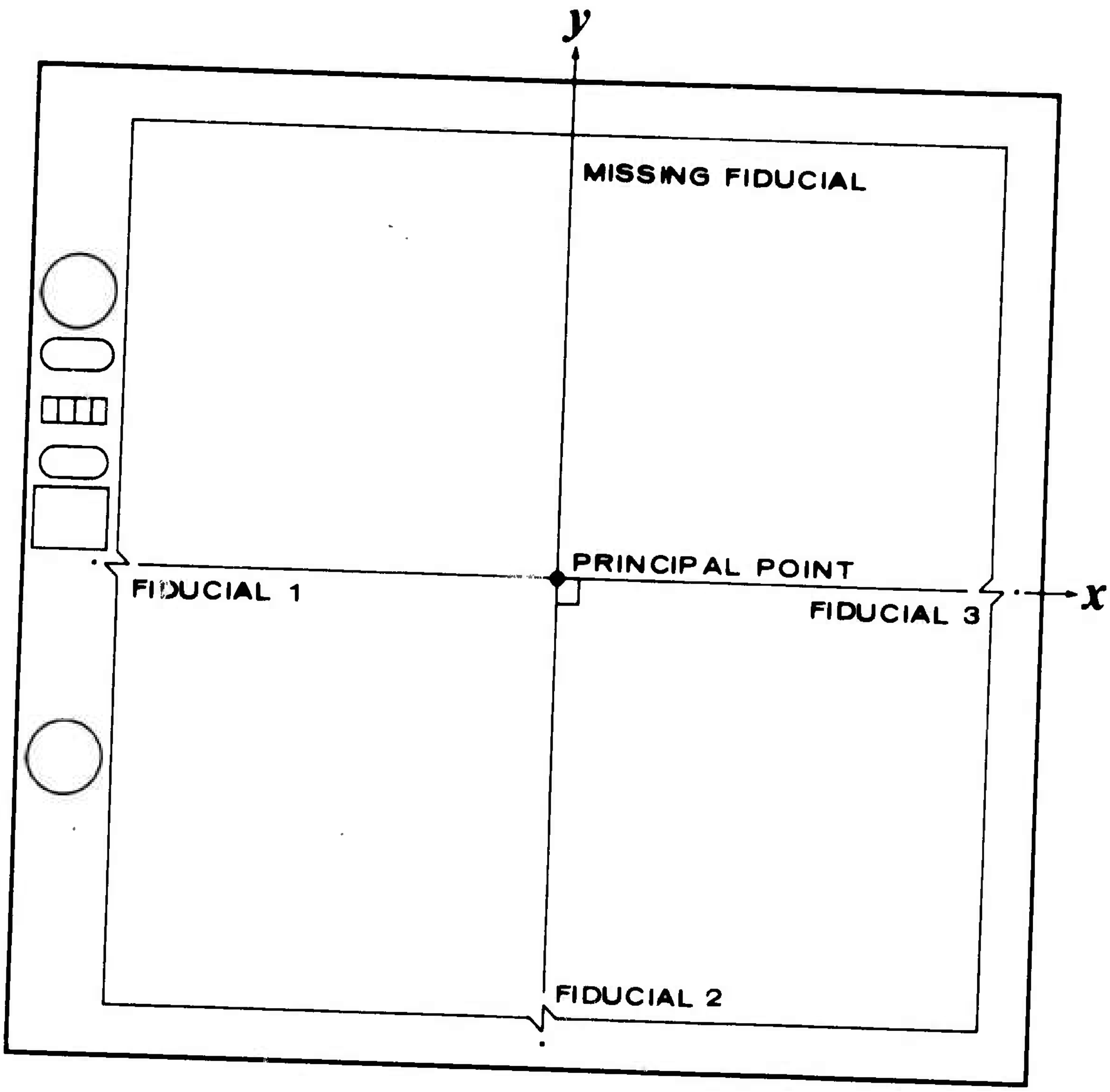

FIGURE 10. PRINCIPAL POINT LOCATION

TABLE I. SUMMARY OF AEROTRIANGULATED STRIPS

Strip ID	Origin of Strip (Sortie 08-61)	Corresponding Radar Strip (Sortie 08-61)	Radar Model Involved	Number of Camera Stations Triangulated	Number of Ground Control Points	Offset Distance to Centerline of Test Area	Average Standard Deviations of Camera Station Coordinates
3	Frame Nos. 52(Last Exposure) through 56(First Exposure)	Pass 3 Channel A	Opposite-Side and Same-Side	10	7	6.6 NM	X:14.4 meters Y:16.6 meters Z:10.2 meters
4	Frame Nos. 69(Last Exposure) through 72(First Exposure)	Pass 4 Channel B	Opposite-Side	9	7	9.2 NM	X:10.6 meters Y:11.7 meters Z: 7.8 meters
5	Frame Nos. 96(First Exposure) through 98(Last Exposure)	Pass 5 Channel A	Same-Side	14	8	18.4 NM	X:12.0 meters Y:12.2 meters Z: 6.3 meters

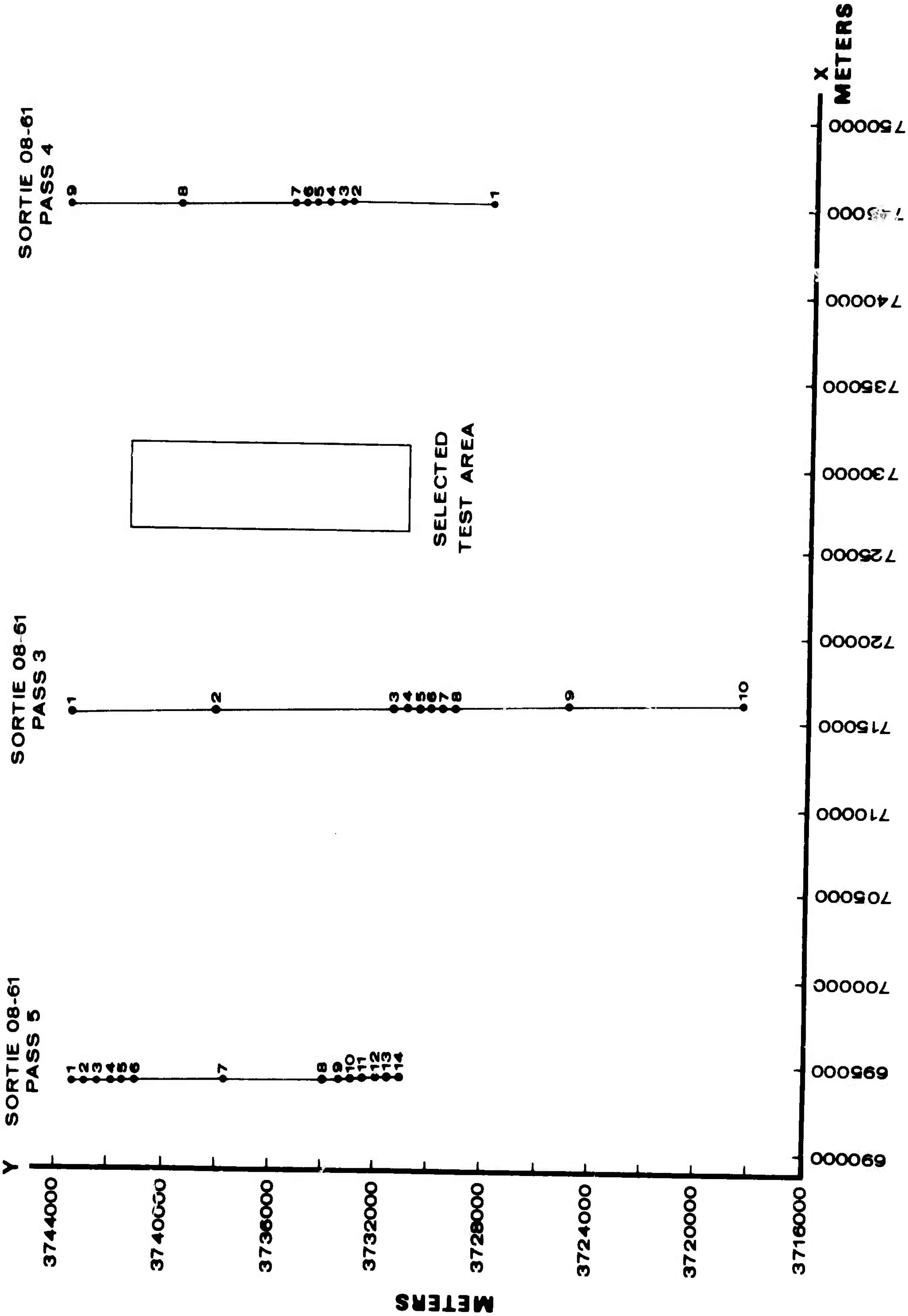

FIGURE 11. CAMERA STATION POSITIONS

2.6 Aerotriangulation of Photography of Test Area (Task 6)

A single model was selected from Sortie 08-212 photography (Frame 2334, seventh exposure; and Frame 2336) for photogrammetric aerotriangulation of test and control points in the test area. The two frames were contact printed onto glass diapositive plates. The images of all points selected on the radar strips in Task 4 were then drilled stereoscopically on the plates with the Wild PUG and measured on the Mann comparator. Additional points lying outside the test area, but within the confines of the photogrammetric model, were selected, drilled, and measured in order to strengthen the model's geometric solution. A total of 74 image points, plus the 3 fiducial marks, were measured on each plate.

Preprocessing of image coordinates was accomplished in accordance with the approach outlined in Section 2.5. Horizontal and vertical control was scaled from two USGS quadrangle maps (1:24,000 scale). In addition to points chosen specifically to control the aerotriangulation, all points selected in Task 4 which were identifiable on the maps were scaled and used as control. A total of 31 horizontal and 13 vertical control points were used. Standard deviations of 12 meters in X and Y and 2 meters in Z (elevation) were assigned to the control for weighting purposes.

The 74 points in the model were photogrammetrically aerotriangulated using the same analytical least squares solution employed for the photography flown simultaneously with the radar. Data reduction, including error propagation, was performed on Autometric's IBM 360/44 computer. The aerotriangulated positions of the points in the test area are given in Table II. It is quite apparent from Table II that there is only modest variation in elevation, the range between highest and lowest points being 90 meters.

The a posteriori variance of unit weight, computed from the least squares solution, indicated a standard deviation of 0.040 mm in the measurement of each image coordinate, in agreement with the value obtained from the aerotriangulation of the photography flown simultaneously with the radar. The error propagation yielded standard deviations of 6.8 meters, 6.7 meters and 8.7 meters in the triangulated X, Y and Z coordinates, respectively. The fit of the triangulated model to the control scaled from the topographic maps resulted in RMS (Root Mean Square) discrepancies of 8.6 meters, 7.3 meters and 7.4 meters in the X, Y and Z-coordinates, respectively.

TABLE II. AEROTRIANGULATED POSITIONS OF POINTS IN TEST AREA

Point No.	Type (See Code)	In Radar Model	UTM Coordinates X (meters)	UTM Coordinates Y (meters)	Elevation Above Mean Sea Level Z (meters)
1	A	I,II	729472.3	3730913.7	301.1
2	A	I,II	729561.3	3731481.3	307.4
3	A	I,II	729643.2	3731973.8	294.6
4	A	I,II	729426.8	3731979.3	290.4
5	A	I,II	729185.4	3732608.7	282.8
6	A	I,II	728385.1	3733029.4	300.5
7	A	I	727670.7	3732582.9	266.6
8	A	I	726558.1	3732783.9	278.6
11	B	I	727280.7	3733179.3	259.2
12	A	I	727575.8	3733319.8	278.2
13	A	I,II	727920.8	3733186.0	271.7
14	A	I	728984.5	3736560.7	253.9
15	A	I	728023.9	3736555.5	251.0
16	A	I	727096.9	3736604.2	245.8
17	A	I	727316.1	3737168.7	251.4
18	A	I	726915.9	3737138.8	234.8
19	C	I,II	729338.8	3738427.5	242.4
20	A	I	728706.0	3738204.0	242.4
21	C	I	728205.0	3738142.6	241.5
22	C	I	727281.0	3737892.5	228.4
23	D	I	726573.4	3737973.4	217.2
24	A	I,II	728166.5	3733486.6	286.7
25	A	I,II	728555.2	3733431.5	286.8
26	E	I,II	728781.5	3734005.2	259.6
27	A	I	727898.0	3739014.1	218.4
28	A	I	726389.6	3738892.9	236.8
29	A	I	726697.7	3739399.7	223.1
30	A	I	727550.9	3739729.1	225.5
31	A	I	726939.2	3739853.4	222.4
32	A	I	727244.7	3740138.0	237.9
33	A	I	726331.6	3740824.3	302.7
34	A	I	728039.5	3740226.7	247.3
35	F	I,II	729126.3	3740745.1	236.1
36	C	I	728468.9	3739254.2	219.6
38	G	I,II	727951.4	3738558.2	234.5
39	A	I,II	727747.4	3740654.3	263.[illegible]
43	F	I	728714.8	3734158.3	257.0
44	A	I,II	728485.5	3734326.8	258.9
45	A	I,II	727803.9	3735116.3	259.4
46	A	I	727828.4	3735990.1	236.3
48	D	II	730662.0	3734571.6	245.0
49	B	I,II	729356.8	3736719.6	238.6
50	B	I,II	729599.1	3736794.6	239.2
51	A	II	729904.5	3736691.8	257.0
53	A	II	730188.2	3737470.5	254.4
57	G	I,II	728879.3	3740290.6	244.3
58	E	II	730103.1	3740607.5	260.6
59	D	II	730682.9	3740541.0	248.1
61	A	I,II	728650.9	3740803.5	250.6
62	A	I,II	728345.9	3740673.4	255.6
63	F	I,II	728600.9	3740199.3	236.2
64	A	I,II	728930.5	3739990.5	234.7
90	A	I,II	728457.6	3730973.6	301.7
96	A	I,II	727994.7	3734426.4	277.0

Code:
- A Road Intersection
- B Point of Land in Lake
- C Building Corner
- D Intersection of Road and Drainage Feature
- E Point of Trees
- F Wooded Fence Corner
- G Cupola on Building

2.7 Radar Data Processing (Task 7)

2.7.1 Preliminary Stereo Radar Test Runs

Since the quality of the test material was less than originally anticipated, and lack of certain data required adoption of a special approach for radar data processing, there was considerable doubt that test point positions determined by stereo radar intersection under these conditions would be meaningful. With this uncertainty associated with the project, it was decided to make preliminary stereo radar test runs as soon as possible in order to verify the adopted data reduction procedure and determine the order of accuracy which might be expected in the radar intersected test point positions. The preliminary results could also be used as a basis for deciding whether or not to continue with the project.

Five preliminary runs were first made for Stereo Radar Model I (opposite-side case). The runs varied with respect to the number of terms used in the slant range and time polynomials, and with respect to the number of ground points used for control. The runs revealed that the quadratic term could be dropped from the slant range polynomial without any significant loss in accuracy, and the number of control points could be reduced considerably with very little loss in accuracy. Most important, however, was the encouraging revelation that the data reduction procedure worked and the general level of accuracy of the radar intersected test point positions was surprisingly good. Comparison of the radar intersected test point positions with corresponding aero-triangulated positions resulted in RMS (Root Mean Square) discrepancies which varied from 7.6 to 9.6 meters in X, 9.8 to 20.1 meters in Y, and 11.0 to 19.3 meters in Z.

A sixth preliminary run was made for Stereo Radar Model II (same-side case), with resulting RMS of discrepancies for the test points of 13.0 meters in X, 12.9 meters in Y, and 20.1 meters in Z.

These initial results were reviewed by Government representatives on January 30, 1970. It was felt that the results were sufficiently encouraging to warrant continuation of the project to completion.

Additional preliminary runs for both stereo radar models were made to check the accuracy using very few control points, and to edit out any bad data. The accuracy held up remarkably well when very few control points were used, and only four points exhibited gross discrepancies in one or more of their coordinates. Three of the bad points (#27, #61, and #90) appeared in Model I; two of the points (#58 and #90) were in Model II. These points were rejected from further consideration, leaving 46 points in Model I and 28 points in Model II for control and testing.

The stage was now set for organizing a series of final test runs.

2.7.2 Final Stereo Radar Test Runs

The final stereo radar test runs were organized for the purpose of revealing the effects, if any, of variation in the reduction technique, variation in control point configuration, and variation in radar image coordinate weighting.

Variation in the reduction technique was made with respect to definition of the radar flight path, evaluation of the B_{SR}-coefficient in the slant range calibration, and definition of the zero-Doppler line. The radar flight path for each strip was defined either by a set of line segments connecting successive camera stations, as given in Section 2.3.1, or by a single straight line between the first and last camera stations. The slant range calibration was based upon whether the B_{SR}-coefficient, appearing in Equation (7) (Section 2.3.3), was determined separately for each record, or from all three records combined. (The C_{SR}-coefficient was dropped from the polynomial in accordance with results of the preliminary test runs which indicated that the quadratic term was unnecessary). The zero-Doppler line was defined either normal to the flight path, as it should be, or normal to the ground track, as a simplified model might have it.

Four distinct control point configurations, shown in Figure 12, were employed in the final test runs. Basically, 14 points, distributed fairly evenly over the test area, were selected as the control points for both stereo radar models (Model I: Opposite-side case; and Model II: Same-side case). In Configuration (A), all 14 points were used to calibrate slant range and correlate "time". In Configuration (B), all 14 points were again used for the slant range calibration, but only 2 of these points, one near each end of the test area, were used to correlate "time". In Configuration (C), only 7 of the points were used for the slant range calibration and the "time" correlation. Three points were selected at each end of the test area, and the 7th point was located near the middle of the area. In Configuration (D), only 4 points, two at each end of the test area, were used to calibrate slant range, while 2 of these points (the same 2 used in Configuration (B)) were used to correlate "time".

For the most part, weighting of the radar image coordinates, R_I and T_I, was uniform; that is, a standard deviation of 0.050 mm was assigned to each R_I and to each T_I. For one test run, however, R_I was heavily weighted (assigned standard deviation = 0.0001 mm), while the weight of T_I remained unchanged (0.050 mm); for another test run, T_I was heavily weighted, while the weight of R_I remained unchanged.

The series of final stereo radar test runs is comprised of 11 runs for each of Stereo Radar Models I and II. The parameters for each of the 11 runs are listed in Table III.

Since 14 points were selected for control, 32 points remained in Model I and 14 points remained in Model II as test points.

The computer programs 1 through 4, described in Section 2.3.7, were used in sequence to process the series of test runs. Then, for

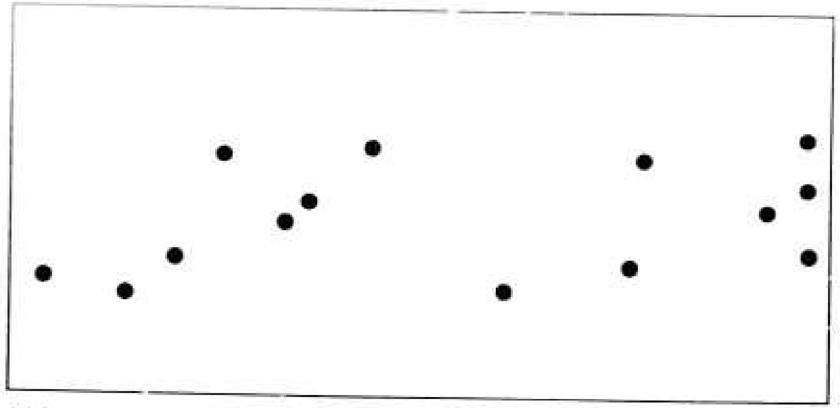

(A) 14 POINTS FOR SLANT RANGE CALIBRATION
AND FOR TIME CORRELATION

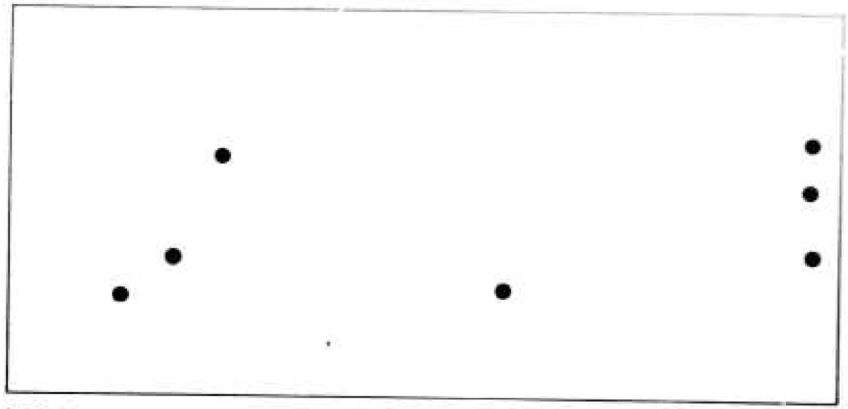

(C) 7 POINTS FOR SLANT RANGE CALIBRATION
AND FOR TIME CORRELATION

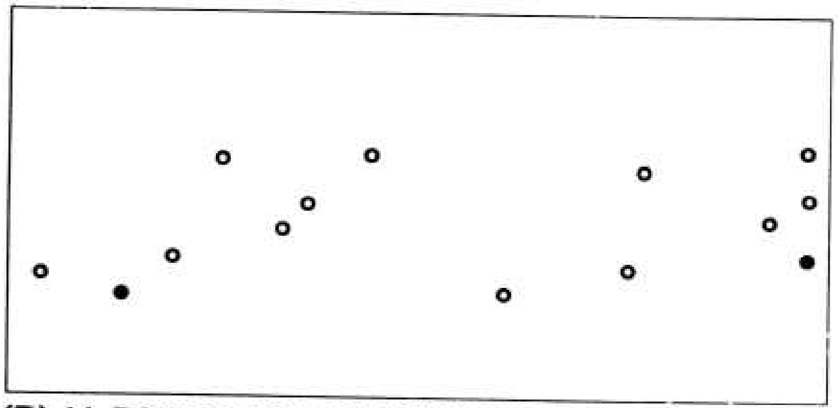

(B) 14 POINTS FOR SLANT RANGE CALIBRATION
AND 2 POINTS FOR TIME CORRELATION

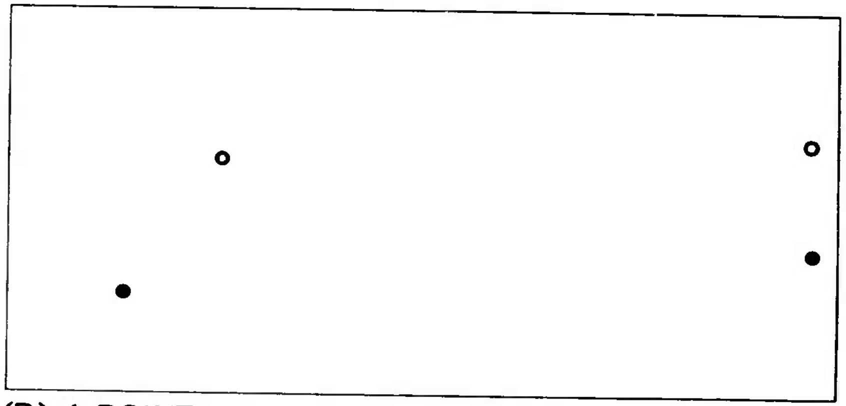

(D) 4 POINTS FOR SLANT RANGE CALIBRATION,
2 POINTS FOR TIME CORRELATION

● USED FOR SLANT RANGE CALIBRATION
AND TIME CORRELATION

○ USED FOR SLANT RANGE CALIBRATION ONLY

FIGURE 12. CONTROL POINT CONFIGURATIONS

TABLE III. PARAMETERS FOR THE FINAL STEREO RADAR TEST RUNS

Run No.	Reduction Techniques			Ground Control			Weights of Image Coordinates R_I & T_I
	Flight Path	Evaluation of B_{SR}	Zero-Doppler Defined Normal To	Configuration	Points for Slant Range Calibration	Points for Time Correlation	
1	Segmented	Separate	Flight Path	A	14	14	Equal
2	Segmented	Combined	Flight Path	A	14	14	Equal
3	Straight Line	Separate	Flight Path	A	14	14	Equal
4	Straight Line	Combined	Flight Path	A	14	14	Equal
5	Straight Line	Combined	Ground Track	A	14	14	Equal
6	Straight Line	Combined	Flight Path	B	14	2	Equal
7	Straight Line	Combined	Flight Path	C	7	7	Equal
8	Straight Line	Combined	Flight Path	D	4	2	Equal
9	Straight Line	Combined	Ground Track	D	4	2	Equal
10	Straight Line	Combined	Flight Path	A	14	14	R_I heavily weighted
11	Straight Line	Combined	Flight Path	A	14	14	T_I heavily weighted

each test run, the final radar intersected positions of the test points were compared with the corresponding aerotriangulated positions (Table II), and the RMS discrepancies were computed for each of the three coordinates, X(across-track), Y(along-track), and Z(elevation). The RMS values are documented later in Section 2.8.

2.7.3 Fit of Radar Records to Ground Points

In addition to determining planimetric position and elevation from a pair of radar records using stereo radar techniques, it is also possible to determine planimetric position, but not elevation, directly from a single record. This approach is, of course, not as rigorous as the stereo radar approach, since it does not account for the effects of relief displacement. However, in view of the modest relief actually exhibited in the selected test area (about 90 meters maximum), it was felt that relief displacement would not be very detrimental.

Essentially, what is done is to fit the radar record to the aerotriangulated positions using a coordinate transformation. If the radar record is indeed a faithful geometrical representation, in plan, of the terrain it is recording, then a good fit should result. Otherwise, large residuals will occur at the fitted points.

Since the radar records for this project are presented in slant range, conversion to ground range presentation is necessary before a faithful planimetric representation of the terrain can be obtained. Ground ranges were computed using the following equation:

$$GR_I = \left[\left(\frac{A_{SR}}{B_{SR}} + R_I\right)^2 - \left(\frac{H}{B_{SR}}\right)^2\right]^{\frac{1}{2}} . \qquad (16)$$

In Equation (16), GR_I is the ground range presentation at image scale; R_I is the plate coordinate, as computed from Equation (5), Section 2.3.3; H is the flying height above terrain, given by the aerotriangulation of the photography flown simultaneously with the radar; and A_{SR} and B_{SR} are parameters of the slant range calibration polynomial (Equation (7) in Section 2.3.3).

Although the slant range presentation is not really a faithful planimetric representation of the terrain, it was decided to include fitting the slant range presentation to the ground control anyway to see how much it affected the fit. Hence, both ground range and slant range presentations are fitted.

Two different coordinate transformations were used for fitting the data. The first transformation is given by Equation (17):

$$\begin{bmatrix} X_I \\ Y_I \end{bmatrix} = \lambda \begin{bmatrix} \cos\phi & \sin\phi \\ -\sin\phi & \cos\phi \end{bmatrix} \begin{bmatrix} R \\ T_I \end{bmatrix} + \begin{bmatrix} K_1 \\ K_2 \end{bmatrix} . \qquad (17)$$

This is a 4-parameter transformation; the 4 parameters are an overall scale factor, λ, a rotation, ϕ, and two translation constants, K_1 and K_2. R_I and T_I are the plate coordinates of the radar image of point I, as computed from Equations (5) and (6), respectively; and X_I and Y_I are the across-track and along-track ground coordinates, respectively.

The second transformation which was used is a 6-parameter transformation, given by Equation (18):

$$\begin{bmatrix} X_I \\ Y_I \end{bmatrix} = \begin{bmatrix} \cos\phi & \sin\phi \\ -\sin\phi & \cos\phi \end{bmatrix} \begin{bmatrix} \lambda_R & 0 \\ 0 & \lambda_T \end{bmatrix} \begin{bmatrix} 1 & \sin\eta \\ 0 & \cos\eta \end{bmatrix} \begin{bmatrix} R_I \\ T_I \end{bmatrix} + \begin{bmatrix} K_1 \\ K_2 \end{bmatrix} \qquad (18).$$

In this transformation, two distinct scale factors, λ_R and λ_T, are employed for scaling R_I and T_I, respectively; and a sixth parameter, η, accounts for non-orthogonality of the R_I and T_I axes.

All ground points measured in each radar record and used in the stereo radar test runs were used for fitting the record to the aerotriangulated positions. Specifically, 52 ground points were used to fit Strip 3 to the aerotriangulated positions, 46 ground points were used to fit Strip 4, and 28 ground points were used to fit Strip 5.

Altogether, four runs were made for each radar strip. Table IV indicates what was done for each run.

TABLE IV. FIT OF RADAR RECORDS TO GROUND POINTS

Run No.	Presentation of Radar Imagery	Type of Transformation
1	Uncorrected Slant Range	4-Parameter
2	Uncorrected Slant Range	6-Parameter
3	Corrected to Ground Range	4-Parameter
4	Corrected to Ground Range	6-Parameter

In each case, the residuals at the ground points were determined, and RMS values for X and Y were computed from the residuals. The RMS values are shown in Table X, Section 2.8.2.

2.8 Analysis of Results (Task 8)

2.8.1 Topographic Accuracy of Stereo Radar

The results of the final stereo radar test runs, the parameters of which are indicated in Table III, are given in Table V. These results consist of RMS values in X, Y and Z for each of the two stereo radar models, computed from discrepancies between the radar determined positions and corresponding aerotriangulated positions. For Stereo Radar Model I, the RMS values are based upon 32 test points; for Stereo Radar Model II, the RMS values are based upon 14 test points.

TABLE V. RESULTS OF THE FINAL STEREO RADAR TEST RUNS

Run No.	RMS Values					
	Model I: Opposite-side case			Model II: Same-side case		
	X(m)	Y(m)	Z(m)	X(m)	Y(m)	Z(m)
1	11.9	10.0	14.7	10.6	14.7	14.1
2	9.5	9.9	11.0	11.3	14.7	11.8
3	7.4	11.8	13.9	9.0	21.4	16.2
4	7.3	11.8	12.3	8.9	21.5	15.4
5	7.3	11.8	12.3	8.7	21.5	13.5
6	7.3	13.4	12.3	8.9	21.2	15.3
7	6.3	14.1	13.8	8.8	21.8	20.2
8	6.5	13.3	14.8	10.6	21.1	24.8
9	6.5	13.3	14.9	9.9	21.1	22.5
10	7.3	11.8	12.3	8.7	21.4	13.4
11	663.6	9.9	2684.7	1302.1	50.2	3449.9
Average Values (Runs 1-10)	7.7	12.1	13.2	9.5	20.0	16.7

Note: (1) Average RMS values are computed from Runs 1-10.

(2) X is in the across-track direction, Y is in the along-track direction, and Z is elevation.

Except for Run 11, the results are very good and very encouraging, particularly when a considerable portion of the error indicated by these RMS values might be attributed to the standard for comparison (the aerotriangulated positions exhibit RMS errors of 8.6 meters, 7.3 meters, and 7.4 meters in X, Y and Z, respectively, when compared with corresponding map-scaled positions). Average values, representative of the results and computed from all test runs except No. 11, are included at the bottom of Table V. From these averages, two very general remarks can be made:

(1) Model I (Opposite-side case) provides greater accuracy than Model II (Same-side case), particularly in Y, the along-track coordinate.
(2) The X (across-track) coordinate is determined with greater accuracy than the Y and Z coordinates for both Models I and II.

The discrepancies in planimetry for Run 4 are plotted in vector form in Figures 13 (Model I) and 14 (Model II). These figures show how the discrepancies are distributed over the test area, in planimetry at least. It is apparent from these plotted discrepancies that certain systematic effects are present. An attempt was made to ascertain the cause or causes of the systematic effects, but it was without success.

In order to demonstrate the effects, if any, of processing the data under different conditions, the test runs are re-grouped into four specific sequences. The first sequence (Runs 1, 2, 3 and 4) attempts to show the effects of varying the reduction technique in two ways:

(1) The flight path is defined by a set of line segments connecting successive camera air stations, as described in Section 2.3.1; or it is defined as one straight line between the first and last stations.
(2) The B_{SR}-coefficient of the slant range calibration polynomial (Equation (7)) is evaluated separately for each radar pass (3, 4 or 5); or it is evaluated only once using data from all 3 passes combined.

For convenience in making comparisons, the results of this sequence of runs are repeated in Table VI. All parameters other than those under investigation are held fixed (See "Note" under Table VI).

The second sequence (Runs 4, 5, 8 and 9) is designed to show the effect of varying the reduction technique with respect to how the zero-Doppler line is defined; that is normal to the flight path, or normal to the ground track. The results of this sequence are repeated in Table VII. Tests were made using two different ground control configurations, A and D, Figure 12.

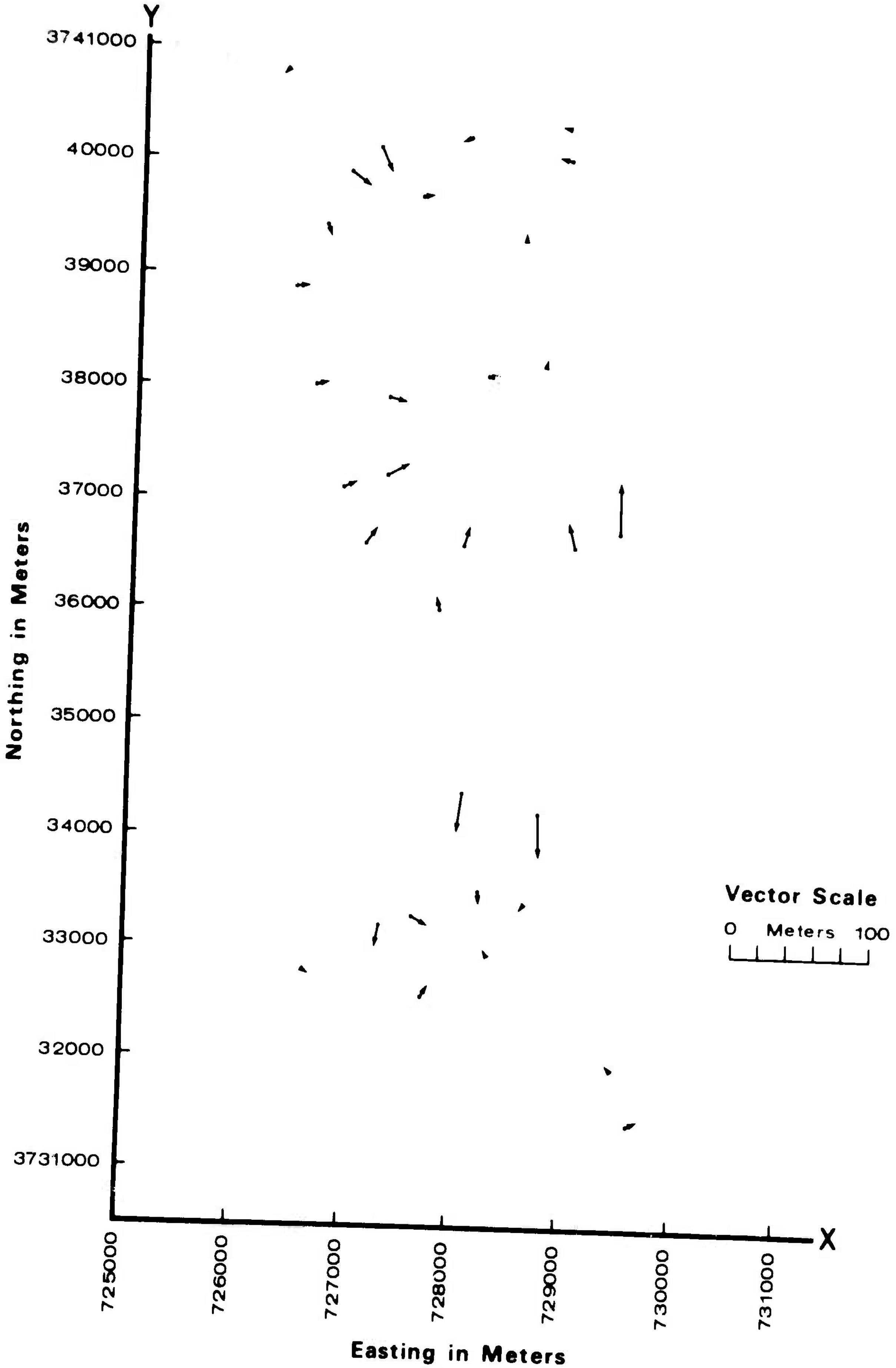

FIGURE 13. DISCREPANCY VECTORS IN PLANIMETRY FOR STEREO RADAR MODEL I (RUN 4).

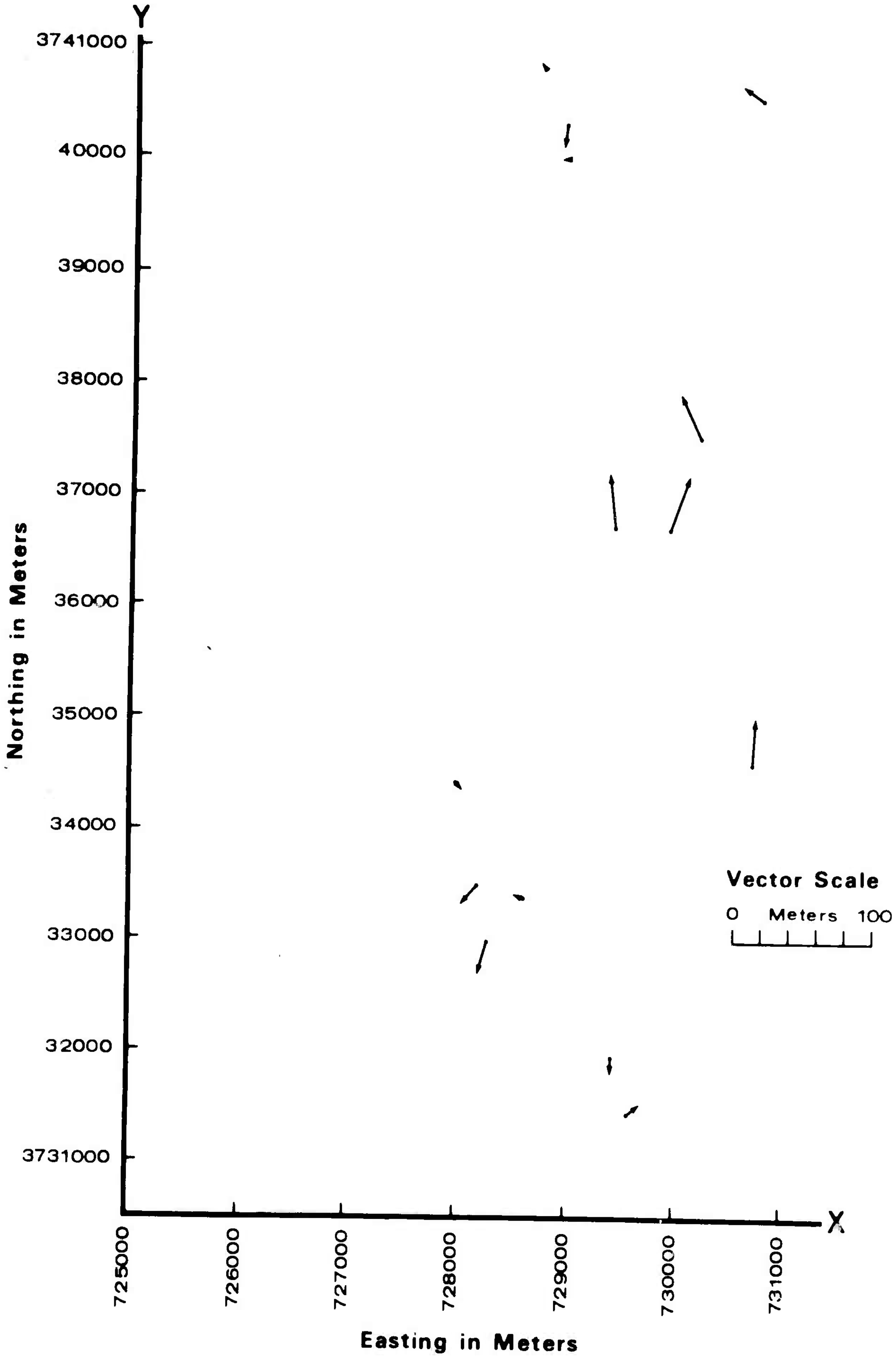

FIGURE 14. DISCREPANCY VECTORS IN PLANIMETRY: FOR STEREO RADAR MODEL II (RUN 4).

TABLE VI. TOPOGRAPHIC ACCURACY OF STEREO RADAR: EFFECT OF FLIGHT PATH DEFINITION AND B_{SR}-COEFFICIENT EVALUATION

Run No.	Flight Path	Evaluation of B_{SR}	RMS VALUES					
			Model I: Opposite-side			Model II: Same-side		
			X(m)	Y(m)	Z(m)	X(m)	Y(m)	Z(m)
1	Segmented	Separate	11.9	10.0	14.7	10.6	14.7	14.1
2	Segmented	Combined	9.5	9.9	11.0	11.3	14.7	11.8
3	Straight Line	Separate	7.4	11.8	13.9	9.0	21.4	16.2
4	Straight Line	Combined	7.3	11.8	12.3	8.9	21.5	15.4

Note: (1) All runs in this table use ground control configuration A (14 points for slant range calibration and for time correlation).

(2) The zero-Doppler line is defined normal to the flight path.

(3) R_I and T_I are equally weighted.

TABLE VII. TOPOGRAPHIC ACCURACY OF STEREO RADAR: EFFECT OF ZERO-DOPPLER LINE DEFINITION

Run No.	Zero-Doppler Line Normal To	Ground Control Configuration	RMS Values					
			Model I: Opposite-side			Model II: Same-side		
			X(m)	Y(m)	Z(m)	X(m)	Y(m)	Z(m)
4	Flight Path	A	7.3	11.8	12.3	8.9	21.5	15.4
5	Ground Track	A	7.3	11.8	12.3	8.7	21.5	13.5
8	Flight Path	D	6.5	13.3	14.8	10.6	21.1	24.8
9	Ground Track	D	6.5	13.3	14.9	9.9	21.1	22.5

Note: (1) Ground control configuration A uses 14 points for slant range calibration and time correlation; configuration D uses 4 points for slant range calibration and 2 for time correlation.

(2) For all runs in this table, the flight path is defined as a straight line, and B_{SR} is evaluated from all 3 records combined.

(3) R_I and T_I are equally weighted.

The third sequence (Runs 4, 6, 7 and 8), repeated in Table VIII, shows the effect of using the different ground control configurations A, B, C and D(See Figure 12), while holding all other parameters constant.

The fourth, and final, sequence (Runs 4, 10 and 11), repeated in Table IX, shows the effect of image coordinate weighting. Again, all parameters other than those under investigation are held fixed.

It is quite evident from the RMS values listed in Tables VI, VII and VIII that no drastic changes in accuracy take place with respect to the variations made in the reduction technique and in the ground control configuration. This, perhaps, should not be too surprising so long as the aircraft flies a straight and level course, the radar equipment remains stable in its image presentation, and the test area is relatively small---conditions which are either true (the test area is indeed small) or very probable.

Nevertheless, there are indications in the tables that the accuracy responds, in part, to some of the changes. For example, Table VI shows that segmentation of the flight path tends to decrease the accuracy of the X-coordinate while improving the accuracy of the Y-coordinate, particularly in Model II; and that the accuracy of the Z-coordinate tends to improve when all 3 radar records are combined to evaluate the B_{SR}-coefficient. Also, Table VIII shows that the accuracy of the Z-coordinate in Model II decreases as fewer ground control points are used for slant range calibration.

Notwithstanding the relative smallness of the test area used in this study, it is still heartening to observe in Table VIII that the few ground points used in Configuration D do about as good a job for Radar Model I as all 14 points used in Configuration A, and it is only in the Z-coordinate of Model II that any deterioration in accuracy takes place. Indeed, it seems remarkable that such accuracy as indicated for Run 8 has been achieved by using only 4 control points, particularly when much of the error could be attributed to the aerotriangulated positions used as the standard for comparison.

It is quite obvious from Table IX that heavily weighting the R_I image coordinate has very little effect, if any, on accuracy, perhaps a slight improvement in the Z-coordinate of Model II. On the other hand, heavily weighting the T_I image coordinate is disastrous. This severe loss of accuracy results from enforcing the intersection of the two zero-Doppler lines (which lie in near-parallel planes) at the expense of the relatively well-determined slant ranges. Actually, there is no good reason in evidence at this time to weight the R_I and T_I image coordinates unequally. Hence, the Run 11 results, although interesting, are of little consequence.

2.8.2 Geometric Analysis

The results of fitting the separate radar records to the aerotriangulated positions, as described in Section 2.7.3, are given in Table X. The first portion of this table repeats the information already given in Table IV.

TABLE VIII. TOPOGRAPHIC ACCURACY OF STEREO RADAR: EFFECT OF VARIOUS GROUND CONTROL CONFIGURATIONS

Run No.	Ground Control			RMS Values					
	Configuration	Points for Slant Range Calibr.	Points for Time Correlation	Model I: Opposite-side			Model II: Same-side		
				X(m)	Y(m)	Z(m)	X(m)	Y(m)	Z(m)
4	A	14	14	7.3	11.8	12.3	8.9	21.5	15.4
6	B	14	2	7.3	13.4	12.3	8.9	21.2	15.3
7	C	7	7	6.3	14.1	13.8	8.8	21.8	20.2
8	D	4	2	6.5	13.3	14.8	10.6	21.1	24.8

Note: For all runs in this table, the flight path is defined as a straight line, the B_{SR}-coefficient is evaluated from all 3 records combined, the zero-Doppler line is defined normal to the flight path, and the weights of R_I and T_I are equal.

TABLE IX. TOPOGRAPHIC ACCURACY OF STEREO RADAR: EFFECT OF IMAGE COORDINATE WEIGHTING

Run No.	Weights of Image Coordinates R_I and T_I	RMS Values					
		Model I: Opposite-side			Model II: Same-side		
		X(m)	Y(m)	Z(m)	X(m)	Y(m)	Z(m)
4	Equal	7.3	11.8	12.3	8.9	21.5	15.4
10	R_I heavily weighted	7.3	11.8	12.3	8.7	21.4	13.4
11	T_I heavily weighted	663.6	9.9	2684.7	1302.1	50.2	3449.9

Note: For all runs in this table, the flight path is defined as a straight line, the B_{SR}-coefficient is evaluated from all 3 records combined, the zero-Doppler line is defined normal to the flight path, and ground control configuration A is used.

TABLE X. RESULTS OF FITTING RADAR RECORDS TO GROUND POINTS

Run No.	Presentation of Radar Imagery	Type of Transformation	RMS Values					
			Strip 3		Strip 4		Strip 5	
			X(m)	Y(m)	X(m)	Y(m)	X(m)	Y(m)
1	Uncorrected Slant Range	4-parameter	198.2	59.7	118.6	47.7	27.8	34.3
2	Uncorrected Slant Range	6-parameter	24.9	12.4	15.4	20.0	10.0	29.4
3	Corrected to Ground Range	4-parameter	17.7	14.3	14.8	20.3	11.3	34.6
4	Corrected to Ground Range	6-parameter	16.1	12.4	13.5	20.0	10.1	29.4

As might be expected, Table X indicates a very poor fit of the radar imagery to the aerotriangulated positions when uncorrected slant ranges and a 4-parameter transformation are used, particularly in the X (across-track, or slant range) direction for Strips 3 and 4. For Strip 5, the fit in X is much better, reflecting the closer agreement between slant range and ground range at the greater offset distance (18.4 NM, as compared to 6.6 NM and 9.2 NM for Strips 3 and 4, respectively).

Table X also shows that the fit is tremendously improved when a 6-parameter transformation is employed, even when slant ranges remain uncorrected. This improvement takes place because the 6-parameter transformation can accommodate, in an average sense, the difference in scale in X between slant range and ground range, while at the same time independently fitting to the "time" scale in Y. The ability of the 6-parameter transformation to account for non-orthogonality of coordinate axes may also contribute to the improvement.

For Strip 5, use of a 6-parameter transformation with uncorrected slant ranges results in a fit every bit as good as the one using corrected ground ranges, reflecting the very small change in slant range scale with respect to ground range at the large (18.4 NM) offset distance.

Quite naturally, Table X indicates considerable improvement in the fit after slant range measurements are corrected to ground ranges. This is as it should be, because the fit is made to ground control points which have essentially a "ground range presentation". As might be expected, correction to ground range combined with a 6-parameter transformation gives the best fit of all.

Understandably, the RMS values in X obtained from geometric fits of the separate radar records to ground control are not as small as their stereo radar model counterparts, although, quite honestly, they are not that much worse, particularly after correction is first made to ground range. As mentioned before, the larger RMS values result from the effects of relief displacement. Since only modest relief is present in the test area, the effects are very small.

It is interesting to observe in Runs 2, 3 and 4 of Table X that although the RMS in Y increases with increasing offset distance (offset distances, as already indicated in Table I, are 6.6 NM, 9.2 NM, and 18.4 NM for Strips 3, 4 and 5, respectively) the RMS in X actually decreases. This seems to reflect the decreasing influence of relief displacement on X as the offset distance increases, while at the same time suggesting that the accuracy of slant range measurement is independent of offset distance.

The discrepancies at the individual points are plotted in vector form in Figures 15, 16 and 17 for Strips 3, 4 and 5, respectively. It is clear from these figures that certain systematic effects are exerting influence. However, as with the discrepancies plotted in Figures 13 and 14, attempts to determine the source or sources of the systematic effects were unsuccessful.

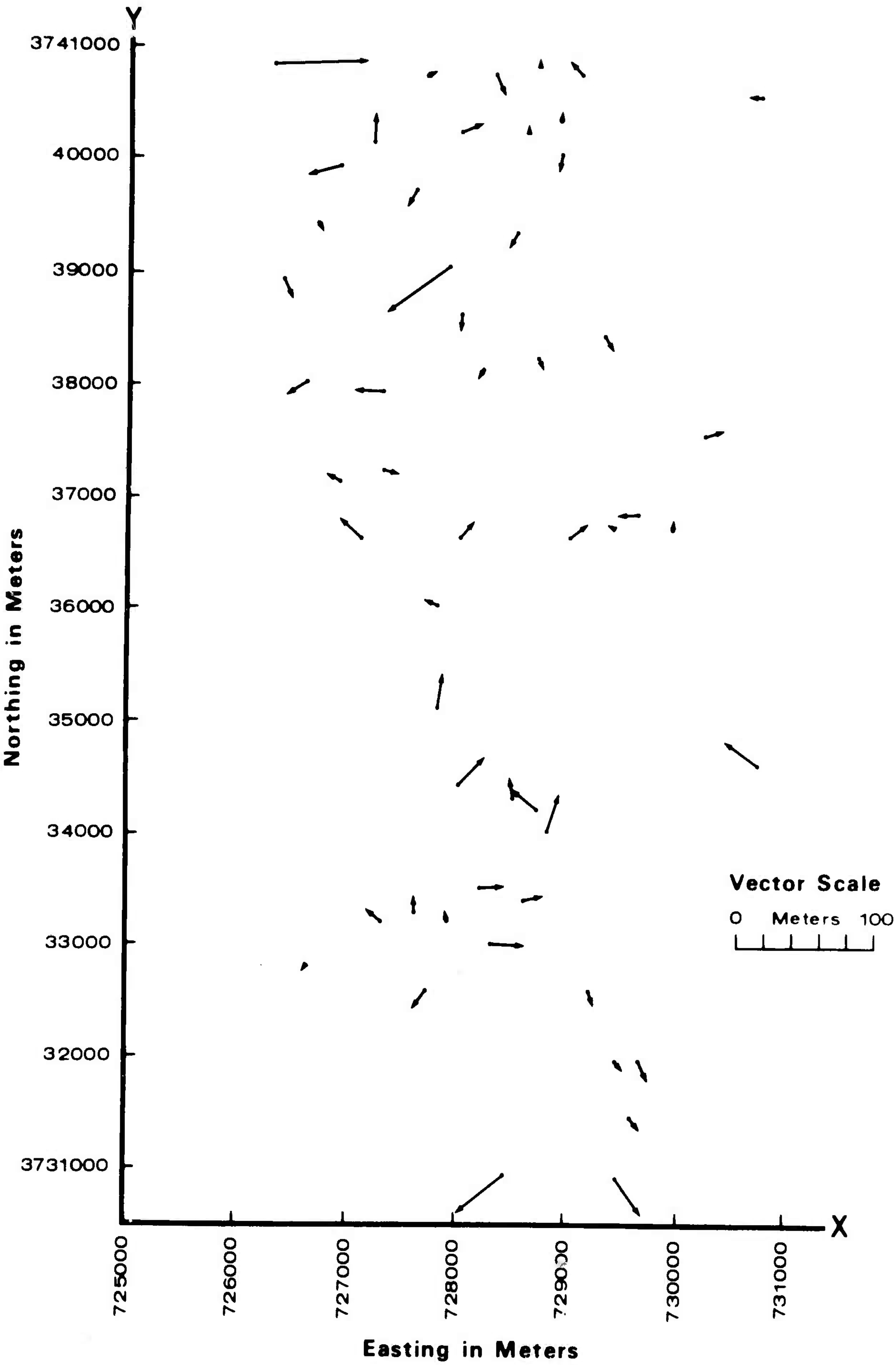

FIGURE 15. DISCREPANCY VECTORS IN PLANIMETRY: IMAGERY FIT FOR RECORD 3.

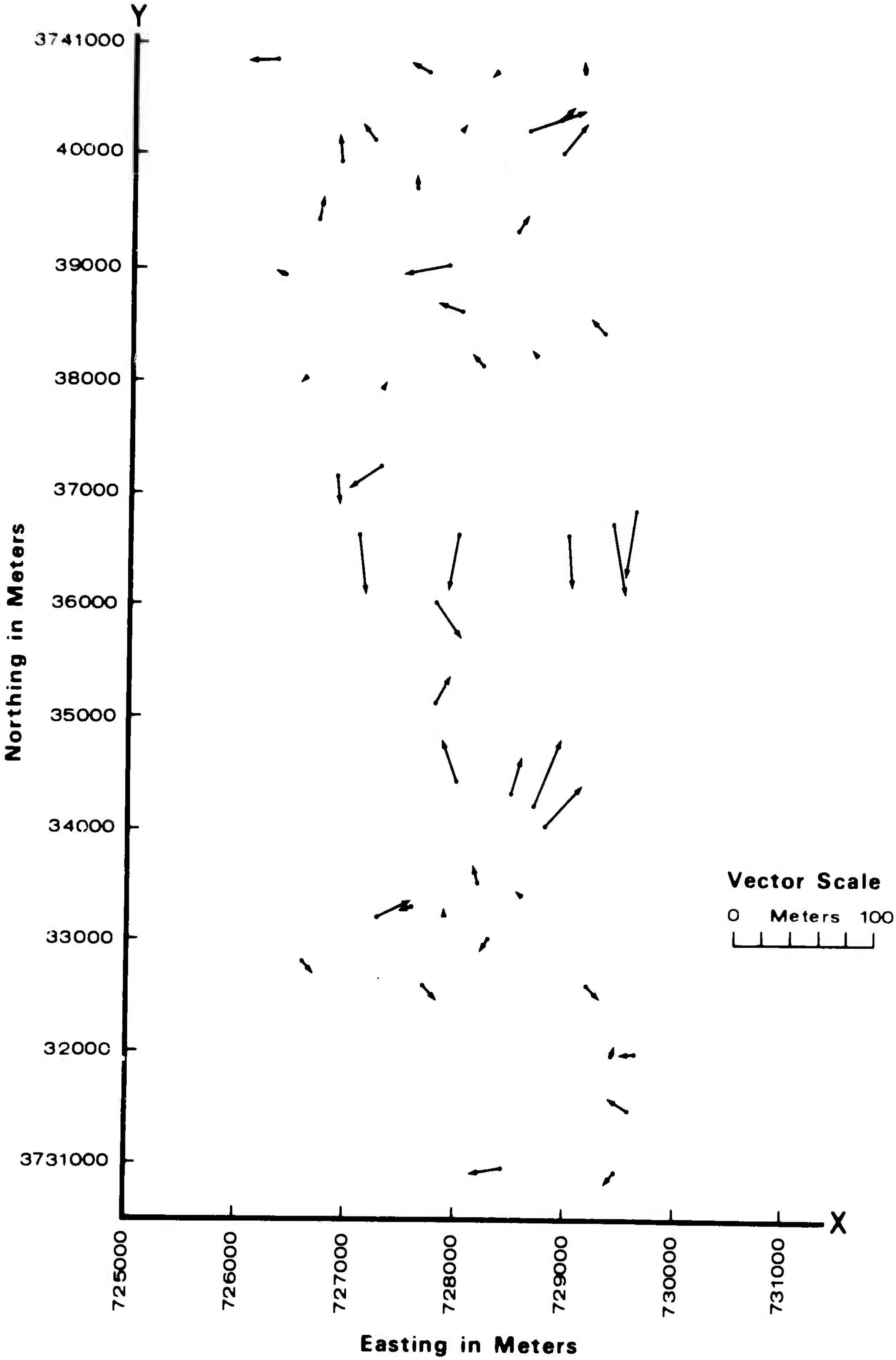

FIGURE 16. DISCREPANCY VECTORS IN PLANIMETRY: IMAGERY FIT FOR RECORD 4.

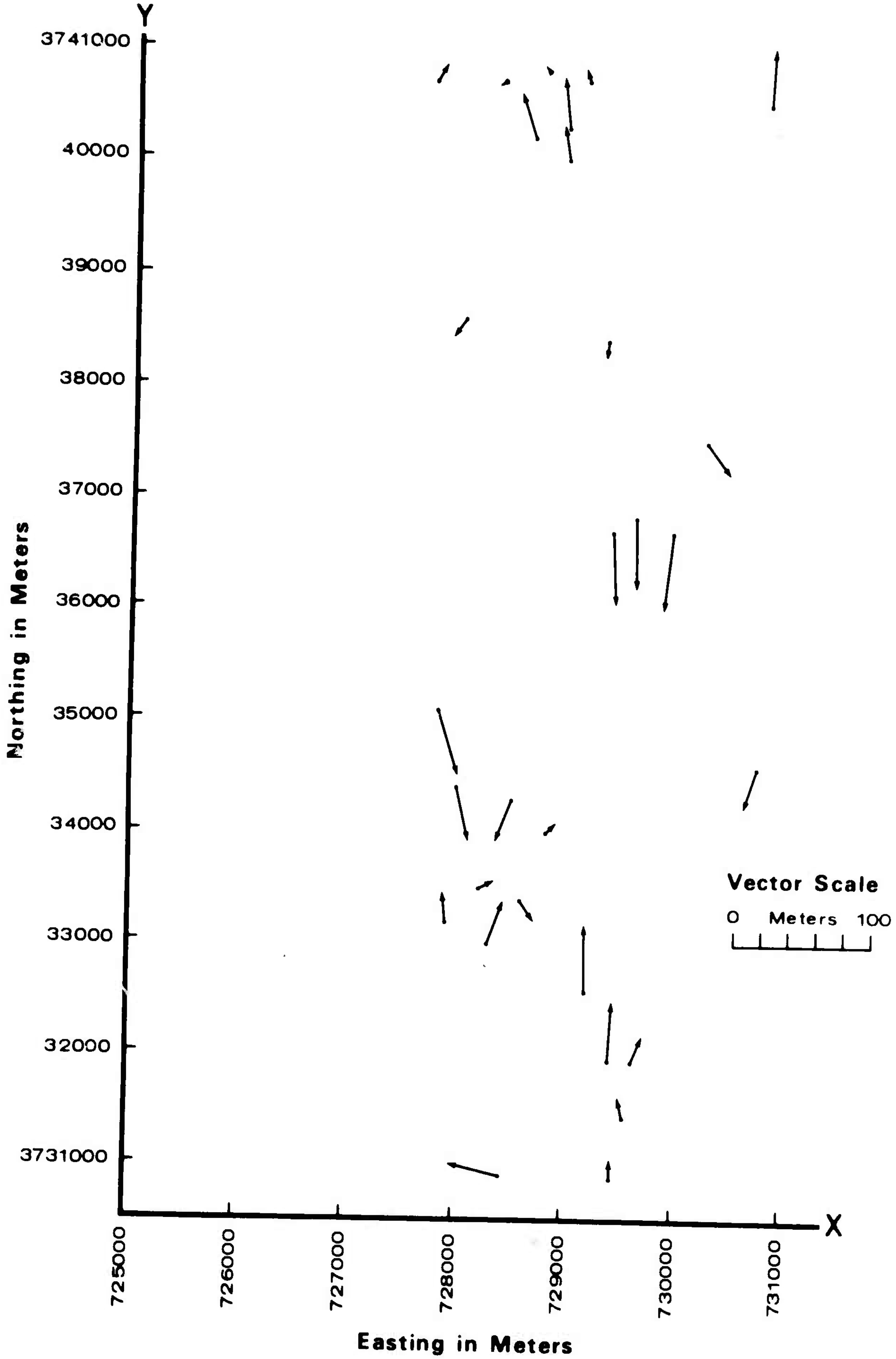

FIGURE 17. DISCREPANCY VECTORS IN PLANIMETRY: IMAGERY FIT FOR RECORD 5.

2.8.3 Slant Range Analysis

The primary function of side-looking radar is to measure slant range. It is of interest, therefore, to check how well this function is being performed.

Slant range calibration curves for a representative test run, Run 4, are plotted in Figure 18. For this run, 14 control points were used for the slant range calibration. Similar, almost identical, graphs can also be plotted for the other test runs. Figure 18 clearly shows the linear relationship between the image coordinate, R_I, and the slant range, indicating a geometrically undistorted presentation of slant range across the radar record, and justifying omission of the quadratic term in the calibration polynomial. Figure 18 also shows the constancy of slope from one record to the next, indicating stability of the radar in recording slant range, and justifying computation of one slope term (the B_{SR}-coefficient) for all three records.

The small, almost imperceptible, departures of the plotted points from the straight lines fitted through them demonstrate the high degree of accuracy which can be achieved in the calibration. RMS values computed from the departures, or residuals, obtained for Test Run 4 are:

Strip 3:	6.4 meters
Strip 4:	13.0 meters
Strip 5:	5.9 meters.

These values are based upon all 14 control points. The other test runs using the same 14 control points for slant range calibration yield essentially the same results. Test runs using fewer control points exhibit much smaller RMS values. However, these smaller values probably resulted from the fewer degrees of freedom in fitting the curves, and so are not given as much credence as the values listed above.

The RMS values for Strips 3 and 5 seem to agree with each other, and are quite reasonable in light of the accuracies obtained for the radar determined positions, Table V. These two nearly equal values also suggest that slant range accuracy is independent of distance, since the offset distances for Strips 3 and 5 are 6.6 NM and 18.4 NM, respectively. On the other hand, the RMS value for Strip 4 seems excessive, and without any apparent reason. Certainly, radar image quality cannot be blamed, for, in this respect, Strip 4 is best.

2.8.4 Error Propagation Results

The error propagation procedure, described briefly in Section 2.3.6, was used to compute standard deviations in X, and Z for each test point position determined by stereo radar intersection. The error propagation was based upon a standard deviation of 0.050 mm assigned to each radar image coordinate. The standard deviations were averaged so as to provide measures of precision which would be typical of the entire test area. These averaged values are given in Table XI.

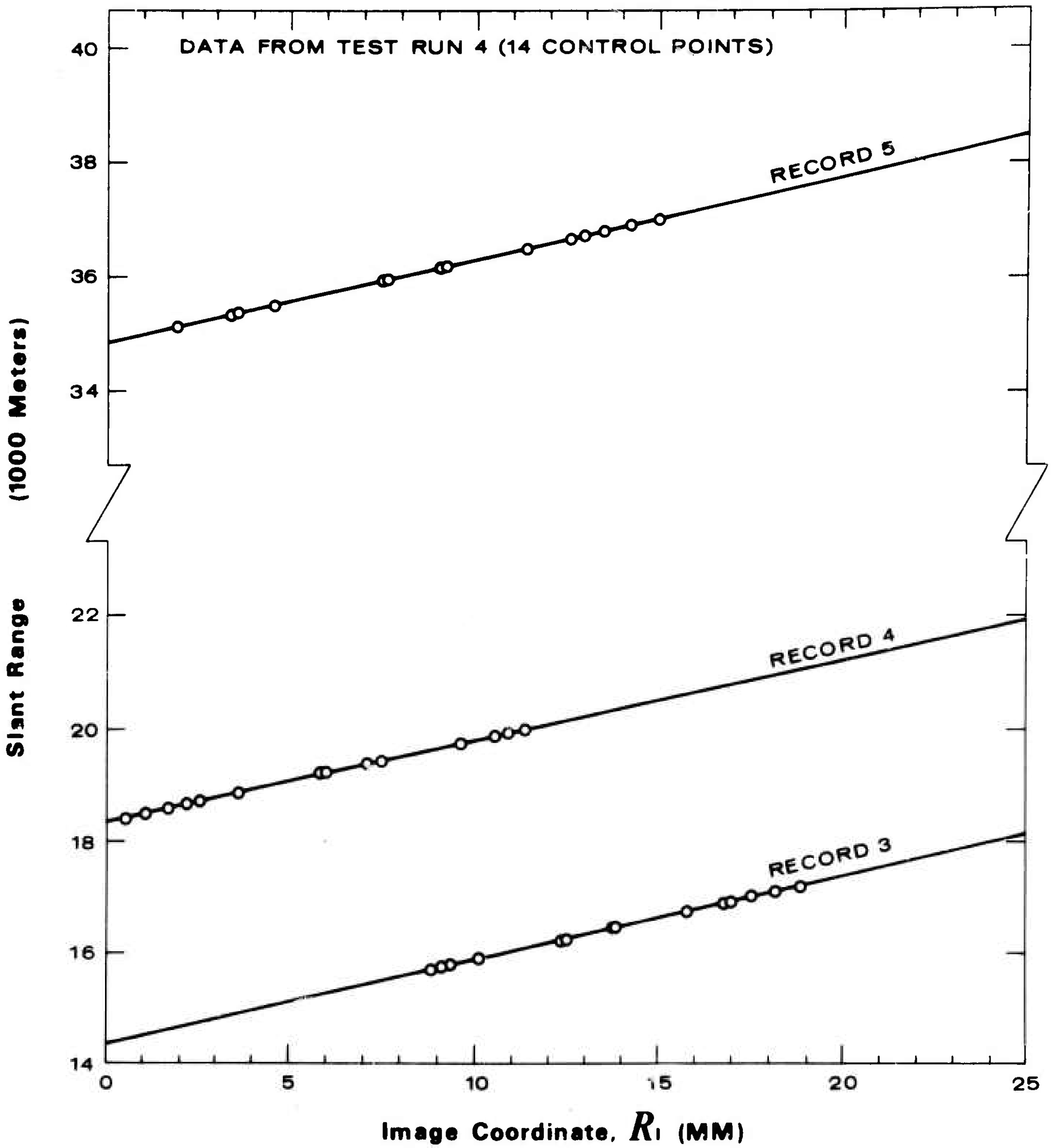

FIGURE 18. SLANT RANGE CALIBRATION CURVES

TABLE XI. STEREO RADAR TEST POINT PRECISION

Stereo Radar Model	Averaged Standard Deviations		
	σ_X(m)	σ_Y(m)	σ_Z(m)
Model I: Opposite-side case	6.3	5.3	9.2
Model II: Same-side case	13.6	5.3	26.5

2.8.5 Applicability of Stereo Radar to Topographic Mapping

Of prime concern in this project is the applicability of the AN/APQ-102(XA-2) side-looking radar to 1:50,000 and 1:250,000 scale topographic mapping, particularly from the standpoint of accuracy. The standards of accuracy for military maps are given in AMS Technical Manual S-1, "Specifications for Military Maps". The standards covering 1:50,000 and 1:250,000 scale topographic maps are repeated herein for convenience.

(1) Class A Maps

(a) Horizontal accuracy: 90% of all planimetric features, except those unavoidably displaced by exaggerated size of symbols, are located within 0.02 inch of their geographical position as referred to the map projection.

(b) Vertical accuracy: 90% of all contours and of all elevations of points interpolated from contours are accurate to within half the basic contour interval.

(2) Class B Maps

Maps that fail to meet the standards of accuracy for Class A, but meet the following standards:

(a) Horizontal accuracy: 90% of all planimetric features, except those unavoidably displaced by exaggerated size of symbols, are located within 0.04 inch of their geographic position as referred to the map projection.

(b) Vertical accuracy: 90% of all contours and of all elevations of points interpolated from contours are accurate to within one contour interval.

(3) Class C-1 Maps

Maps that fail to meet the standards of accuracy for Class B, but meet the following standards:

(a) Horizontal accuracy: 90% of all planimetric features shown, except those unavoidably displaced by exaggerated size of symbols, are located within 0.08 inch of their geographical position as referred to the map projection.

(b) Vertical Accuracy: 90% of all contours and of all elevations of points interpolated from contours are accurate to within two contour intervals.

(4) Class C-2 Maps

Maps that fail to meet the standards of accuracy for Class C-1, but must be retained to fill possible emergency needs, pending replacement.

Applying these standards specifically to 1:50,000 and 1:250,000 scale topographic maps yields the accuracy requirements, in meters, listed in Tables XII and XIII.

Three stereo radar test runs, yielding overall "best", "average", and "worst" accuracies, respectively, were selected from Table V for comparison with the standards of accuracy. Test Run 2, the "best", uses a segmented flight path, 14 control points for slant range calibration and time correlation, and a zero-Doppler line defined normal to the flight path. Test Run 4, the "average", uses a straight line flight path; otherwise, it is the same as Test Run 2. Test Run 9, the "worst" (Test Run 11 was excluded from consideration), uses a straight line flight path, only 4 control points for slant range calibration and 2 for time correlation, and a zero-Doppler line normal to the ground track.

The planimetric errors of the test points were computed from their X and Y components. The percentages of points lying within the standards of horizontal accuracy for Class A and Class B 1:50,000 scale maps, Table XII, were computed for all 3 test runs, and for both stereo radar models. These percentages are listed in Table XIV.

The percentages of points lying within the standards of vertical accuracy for Class A, B and C-1 1:50,000 and 1:250,000 scale maps, Tables XII and XIII, were also computed. These percentages are also listed in Table XIV.

In each instance, the first percentage equal to or exceeding 90% is underlined in Table XIV. From these data, the following statements are made:

(1) Stereo Radar Model I yields sufficient horizontal accuracy for Class A mapping at 1:50,000 scale.
(2) Stereo Radar Model II yields sufficient horizontal accuracy for Class B mapping at 1:50,000 scale, or for Class A mapping at 1:250,000 scale.
(3) Stereo Radar Model I yields sufficient vertical accuracy for Class B mapping at 1:50,000 scale with 20-meter contours, or for Class C-1 mapping at 1:50,000 scale with 10-meter contours, provided ample control is available.
(4) Stereo Radar Model I yields sufficient vertical accuracy for Class A mapping at 1:250,000 scale with 50-meter contours, or for Class B mapping at 1:250,000 scale with 25-meter contours.
(5) Stereo Radar Model II yields sufficient vertical accuracy only for Class C-1 mapping at 1:50,000 scale with 20-meter contours.
(6) Stereo Radar Model II yields sufficient vertical accuracy for Class A mapping at 1:250,000 scale with 50-meter contours, or for Class B mapping at 1:250,000 scale with 25-meter contours, only under the "best" conditions of Test Run 2. Otherwise, Model II can be used only for Class A mapping with 100-meter contours, or for Class B mapping with 50-meter contours, or for Class C-1 mapping with 25-meter contours.

TABLE XII. SPECIFIC STANDARDS OF ACCURACY FOR 1:50,000 SCALE TOPOGRAPHIC MAPS

	Horizontal Accuracy (90% Standard)	Vertical Accuracy (90% Standard)		
		Contour Interval		
		5 meters	10 meters	20 meters
Class A Maps	25.4 m.	2.5 m.	5.0 m.	10.0 m.
Class B Maps	50.8 m.	5.0 m.	10.0 m.	20.0 m.
Class C-1 Maps	101.6 m.	10.0 m.	20.0 m.	40.0 m.

TABLE XIII. SPECIFIC STANDARDS OF ACCURACY FOR 1:250,000 SCALE TOPOGRAPHIC MAPS

	Horizontal Accuracy (90% Standard)	Vertical Accuracy (90% Standard)		
		Contour Interval		
		25 meters	50 meters	100 meters
Class A Maps	127 m.	12.5 m.	25 m.	50 m.
Class B Maps	254 m.	25 m.	50 m.	100 m.
Class C-1 Maps	508 m.	50 m.	100 m.	200 m.

TABLE XIV. PERCENTAGE OF POINTS WITHIN SPECIFIED LIMITS FOR THREE SELECTED TEST RUNS

Stereo Radar Model	Test Run	Horizontal Accuracy		Vertical Accuracy								
		% Points Within		% Points Within								
		25.8 m.	50.8 m.	2.5 m.	5 m.	10 m.	12.5 m.	20 m.	25 m.	40 m.	50 m.	100 m.
		%	%	%	%	%	%	%	%	%	%	%
Model I	2	96	100	18	28	68	71	93	96	100	100	100
Opposite-side case	4	90	100	0	21	56	59	96	96	100	100	100
	9	90	100	18	21	43	53	81	96	100	100	100
Model II	2	85	100	7	21	64	71	85	92	100	100	100
Same-side case	4	71	100	21	28	71	71	85	85	100	100	100
	9	64	100	14	21	42	42	57	64	92	92	100

There is little doubt that the stereo radar, particularly Model I, provides sufficient horizontal accuracy for 1:50,000 and 1:250,000 scale mapping. It is the vertical accuracy which is apparently insufficient in certain cases, and is therefore the controlling factor. In order to portray more graphically what has been said in statements (3) through (6) with respect to vertical accuracy, Tables XV and XVI have been prepared.

Statements (3) through (6), and the accompanying information in Tables XV and XVI, should be accepted with caution, bearing in mind the following qualifications:

(1) The vertical accuracies obtained in the test runs are with respect to well-identified points, measured individually; that is, the points are not interpolated from map contours, as the mapping specifications prescribe.
(2) Comparison was made with aerotriangulated positions which are not entirely error-free themselves. Part of the error assigned to the radar determined positions can thus be attributed to error in the accuracy standard against which comparison was made.
(3) The test area has only modest relief; that is, the testing was done only with moderately hilly terrain, certainly not with mountainous terrain.

The preceding qualifications notwithstanding, the results which have been obtained in this study are very heartening, for they clearly demonstrate a degree of geometrical fidelity in the AN/APQ-102(XA-2) radar that offers much promise for application to 1:50,000 and 1:250,000 scale topographic mapping.

TABLE XV. SUITABILITY OF STEREO RADAR FOR 1:50,000 SCALE TOPOGRAPHIC MAPPING

	Contour Interval		
	5 meters	10 meters	20 meters
Class A Maps	-	-	-
Class B Maps	-	-	I*
Class C-1 Maps	-	I*	I, II

I*: Stereo Radar Model I is suitable, only when ample control is available.
I,II: Stereo Radar Models I and II are suitable.

TABLE XVI. SUITABILITY OF STEREO RADAR FOR 1:250,000 SCALE TOPOGRAPHIC MAPPING

	Contour Interval		
	25 meters	50 meters	100 meters
Class A Maps	-	I,II*	I,II
Class B Maps	I,II*	I,II	I,II
Class C-1 Maps	I,II	I,II	I,II

I,II*: Stereo Radar Model I is suitable; Model II is suitable only under "best" conditions.
I,II: Stereo Radar Models I and II are suitable.

3. DISCUSSION

3.1 Test Material

No particular problems were encountered in sorting out the test material. The lack of any kind of indexing for the vertical photography did, however, make the job of identifying the imagery by strip a tedious one. During the inspection, some of the data were disqualified from consideration as test material:

a) Vertical photography of Strips 1 and 2 for both Sortie 08-61 and Sortie 08-75 was exposed at 60% endlap. Strips having more closely spaced camera stations (more exposures) can better define the flight path for the purpose of the investigation.

b) Radar Pass 6 of Sortie 08-61 had no simultaneous vertical photography.

c) Pass 4 of Sortie 08-75 had no radar imagery.

d) Image quality on four radar strips (08-61, Pass 6; 08-75, Passes 3 and 5; and 08-212, Pass 3) was very poor.

In view of the poor quality of the photography and radar imagery obtained for this investigation, it was decided by Autometric, with the concurrence of ETL, to confine the test to an area smaller than that originally planned. Radar image quality had the largest influence on the selection of test material. Unfortunately, the vertical photography corresponding to the best radar coverage was of poor quality. Radar image quality also influenced the location of the test area, since the size of the test area was limited and image quality varied within the strip.

3.2 Stereoscopic Viewing

During the course of the data inspection, it became doubtful to the investigators that the conjugate radar imagery provided could be visually correlated to the point where stereoscopic parallaxes could be measured directly. Only slight relief was apparent in the same-side radar model, and very little relief, real or imagined, was seen in the opposite-side stereomodel. In fact, for the opposite-side model, a good deal of visual effort was required just to correlate images. When a floating mark was introduced into the model, it was barely possible, if at all, to maintain correlation of imagery and perceive the floating mark simultaneously. This is understandable since the principle of projection in the human eye is different from that of the radar projection. The

absence of noticeable relief, even in the same-side model where images were easily correlated, can then be explained by the difference between visual and radar parallax. The same-side model can be visually correlated because the radar parallaxes are much smaller than those of the opposite-side case and within range of the eyes' capability to fuse conjugate images. However, because of the smaller parallaxes, little relief is seen. In addition, actual ground relief in the area is only 200 to 300 feet, perhaps yielding radar parallaxes too small to have visual significance.

3.3 Data Reduction Approach

Since it was obvious that little could be accomplished using visual stereoscopic methods, the approach in the investigation relied entirely on analytical methods, along the lines of analytical photogrammetry, but through the geometry and conditions imposed by the radar system. The mathematical analysis and programming for the investigation had to incorporate special techniques for calibrating the radar range measurements, establishing an artificial time scale, and correlating time, since all collateral data, such as range marks and time marks, were missing from the radar records. As it turned out, the establishment of missing data in such an empirical manner was quite successful.

In the mathematical analysis, the original thought was to fit time polynomials to the flight path (triangulated camera stations) and interpolate between camera stations for radar positions using second or higher order polynomials. However, with the camera station spacing so varied (400 to over 6000 meters), where the largest spacing represents about 1/2 minute of flying time, it seemed impractical to fit high-order polynomials to the flight path. As a result, linear functions were used to describe the flight paths, with 2 successive camera stations defining each increment of the flight.

3.4 Radar Mensuration

It was originally intended to work with enlarged scale radar imagery (approximately four times negative scale). However, after a visit to the Engineering Topographic Laboratories for the purpose of viewing the enlarged imagery on the Wild STK-1 Stereocomparator, it became evident that the additional enlargement from optical magnification in the instrument degraded the model. Since the Mann Comparator has similar optical magnification, it was decided to use imagery at negative scale.

The major difficulty in the radar mensuration task was the identification of points on the radar imagery. Image quality was lowest in the same-side model where only 30 points were identified for measurement. The opposite-side model provided an adequate total of 49 points.

3.5 Aerotriangulation

Several problems were encountered in the aerotriangulation of the vertical photography taken simultaneously with the radar. The lack of camera calibration parameters made it impossible to compensate for

film distortion, and the minimal fiducial imagery hampered the transformation of comparator measurements to plate coordinates. It was necessary to define the plate coordinate system and assume the location of the principal point from comparator measurements of the three available fiducial marks. The principal point was determined by computing the intersection of the line formed by two of the fiducials (on opposite sides of the plate) and the perpendicular dropped to it from the third fiducial. Master fiducial coordinates were then derived by computing distances from the principal point to each of the measured fiducial images. The values used for preprocessing were based on the mean values computed from measurements on ten frames of Strip 3. Although the master fiducial coordinates derived from Strip 3 were applicable to Strip 4, it was necessary to adjust two of the values by approximately 0.100 mm each for successful preprocessing of Strip 5. This may be an indication of significant film distortion in Strip 5, relative to Strips 3 and 4.

Initial aerotriangulation of each strip was made assuming a 0.010 mm standard deviation for x and y on the plate. The 0.010 mm value was chosen as a starting estimate, although not a very realistic one for the quality of input imposed on the triangulation. As expected, the results of all three strips indicated that the plate coordinate weights should be relaxed by a factor of approximately four. The strips were rerun assuming 0.040 mm standard deviations in the plate coordinates, and results indicated that consistent weighting was used.

3.6 Limitations of This Stereo Radar Analysis

Before concluding this report, a few words should be said about the limitations of this stereo radar analysis.

Firstly, the analysis was conducted using very selective material. Of all the radar imagery acquired for the test, only a small portion, the best of it, was selected for analysis. This, of course, was done purposely to find out what results could be obtained with reasonably decent imagery, and also with the expectation that future imagery would be as good, if not better, than this selected imagery.

Secondly, for reasons given earlier, the selected test area was very small and lacking in mountainous terrain. The smallness of the area limited the number of test points available for selection. Only 49 points were selected for Stereo Radar Model I, and 30 points for Model II, hardly enough from which to draw conclusive results, but nevertheless sufficient to give useful measures of accuracy. The lack of mountainous terrain in the test area precludes drawing any conclusions from this analysis about stereo radar accuracy in this kind of terrain.

Thirdly, there was very little collateral data supporting the radar imagery and aerial photography, thus requiring adoption of a special approach to data reduction. As a consequence, the results are directly related to the particular approach used, and should not be extrapolated, without caution, to other possible stereo radar reduction techniques.

Had collateral data, such as range and time marks, been furnished, there is really no telling what improvements in accuracy, if any at all, would have occurred.

Fourthly, the photogrammetrically triangulated test point positions, used as the standard of comparison for measuring the radar accuracy, were not without error themselves, inhibiting measurement of the true accuracy of the radar.

Finally, the specific test points selected for analysis were well-defined and very carefully identified in the imagery. They were certainly not representative of the myriad of image points that would have to be used for preparation of a topographic map.

In spite of these limitations, this analysis still gives good insight into the accuracy of stereo radar. Quite clearly, it shows that the AN/APQ-102(XA-2) radar has the geometrical fidelity necessary for the construction of topographic maps at 1:250,000 scale and, even possibly, 1:50,000 scale.

4. CONCLUSIONS

From this particular stereo radar analysis, the following conclusions are drawn:

(1) The AN/APQ-102(XA-2) radar does a surprisingly good job of locating well-identified ground points accurately using stereo radar techniques. In general, the opposite-side case (Model I) provides greater accuracy than the same-side case (Model II); and X (the across-track coordinate) is determined with greater accuracy than Y (the along-track coordinate) or Z (the elevation). Specifically, average RMS values of 7.7 meters, 12.1 meters and 13.2 meters in X, Y and Z, respectively, were obtained for Model I; and average RMS values of 9.5 meters, 20.0 meters and 16.7 meters were obtained for Model II.

(2) The geometric fidelity of the AN/APQ-102(XA-2) radar is clearly demonstrated by the excellent fit of the three selected radar records to ground control provided by photogrammetric aerotriangulation. Specifically, the RMS values in X are 16.1 meters, 13.5 meters and 10.1 meters in Strips 3, 4 and 5, respectively; and the RMS values in Y are 12.4 meters, 20.0 meters and 29.4 meters.

(3) The horizontal accuracy provided by the AN/APQ-102(XA-2) radar, using stereo radar techniques, is adequate for all topographic mapping at scales of 1:50,000 and 1:250,000, except perhaps Class A mapping at 1:50,000 scale. Even for this one possible exception, Model I (opposite-side) stereo radar may provide sufficient accuracy.

(4) Vertical accuracy is really the deciding factor with respect to applicability of the AN/APQ-102(XA-2) radar to topographic mapping. For mapping at 1:250,000 scale, the Model I (opposite-side case) vertical accuracy seems sufficient for Class A mapping with 50-meter contours, or for Class B mapping with 25-meter contours. For 1:50,000 scale, the Model I vertical accuracy seems sufficient, only under the best test conditions, for Class B mapping with 20-meter contours, or for Class C-1 mapping with 10-meter contours.

The conclusions just stated, are based upon actual results of the specific tests made in this investigation. It is conceivable that with better imagery, with more collateral data, and with more accurate positions for the standard of comparison, the results could be even better. On the other hand, for a larger test area, with mountainous terrain, the results could be worse. Therefore, it remains to be seen what accuracy

can be obtained over an extended area, with varied relief, using high-quality imagery with all possible collateral data.

If one general conclusion might be drawn from this study, it is this: the AN/APQ-102(XA-2) radar, using stereo radar techniques, particularly with opposite-side configuration, yields enough accuracy to make it a very attractive contender for the job of all-weather, day-night topographic mapping at scales of 1:250,000 and even 1:50,000. Of course, more tests under better controlled conditions will have to be made in order to arrive at any really conclusive results. In the meantime, the results of this test, qualified as they are, clearly point to the potential of this stereo radar technique for topographic mapping.

5. RECOMMENDATIONS

The following two recommendations are made:

(1) More extensive tests with real data should be made, under the conditions originally anticipated for this investigation, and using better ground control, in order to obtain more conclusive results.

(2) Theoretical analyses, using simulated radar data, should be made for the purpose of testing the effects of various errors in the stereo radar model. Such analyses would provide insight into the stereo radar reduction technique with respect to what is and what isn't important.

APPENDIX

MATHEMATICAL FORMULATION

1. DETERMINATION OF RADAR AIR STATION POSITION AND SLANT RANGE FOR A GIVEN CONTROL POINT

Let C_1 and C_2 be two camera stations initiating and terminating a line segment which defines the flight path, Figure A-1. The radar air station, R, is located at the foot of the zero-Doppler line, which is normal to the flight path and passes through the control point I.

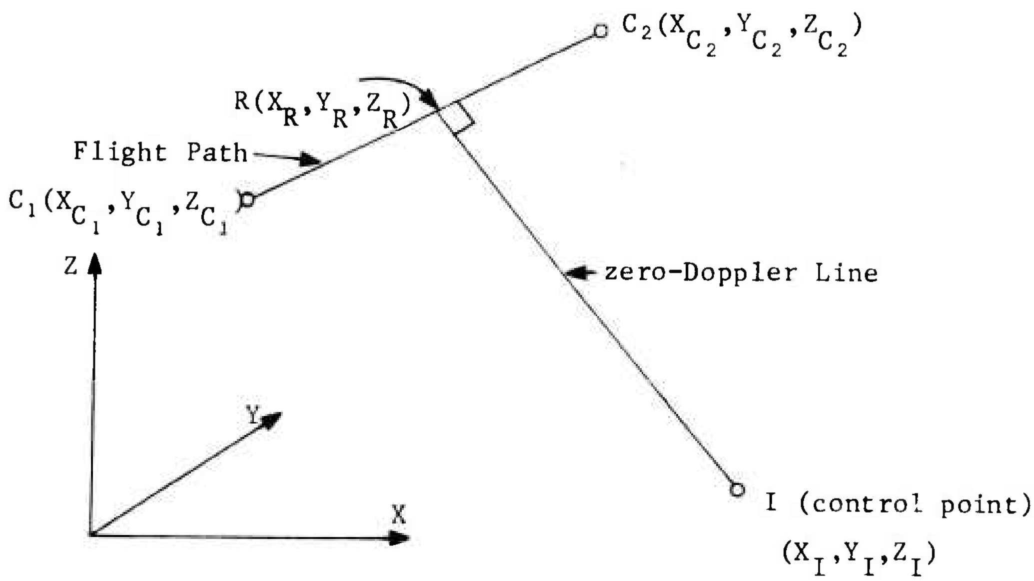

Figure A-1

The direction numbers of the flight path are:

$$\alpha = X_{C_2} - X_{C_1}$$

$$\beta = Y_{C_2} - Y_{C_1}$$

$$\gamma = Z_{C_2} - Z_{C_1}$$

Since the zero-Doppler line is normal to the flight path, it follows that:

$$\alpha(X_R - X_I) + \beta(Y_R - Y_I) + \gamma(Z_R - Z_I) = 0.$$

Also, since the flight path is a straight line,

$$(X_R - X_{C_1}) = \frac{\alpha}{\beta}(Y_R - Y_{C_1})$$

and

$$(Z_R - Z_{C_1}) = \frac{\gamma}{\beta}(Y_R - Y_{C_1}) .$$

These three equations are solved for X_R, Y_R and Z_R, the coordinates of the radar air station. The solution is:

$$X_R = \frac{\alpha S}{\alpha^2 + \beta^2 + \gamma^2} + X_{C_1}$$

$$Y_R = \frac{\beta S}{\alpha^2 + \beta^2 + \gamma^2} + Y_{C_1}$$

$$Z_R = \frac{\gamma S}{\alpha^2 + \beta^2 + \gamma^2} + Z_{C_1}$$

in which

$$S = \alpha(X_I - X_{C_1}) + \beta(Y_I - Y_{C_1}) + \gamma(Z_I - Z_{C_1})$$

Once the position of the radar air station is known, the slant range, SR_I, to the control point I can be computed:

$$SR_I = [(X_R - X_I)^2 + (Y_R - Y_I)^2 + (Z_R - Z_I)^2]^{\frac{1}{2}} .$$

2. SLANT RANGE CALIBRATION

The slant range, SR_I, for control point I is assumed to be a second-order polynomial function of the R_I-coordinate:

$$SR_I = A_{SR} + B_{SR} R_I + C_{SR} R_I^2$$

in which

$$R_I = r_I \cos\theta + t_I \sin\theta.$$

For a least squares solution, the condition equation for control point I is:

$$F_I = A_{SR} + B_{SR}(r_I \cos\theta + t_I \sin\theta) + C_{SR}(r_I \cos\theta + t_I \sin\theta)^2 - SR_I = 0 .$$

In this equation, SR_I is the "observed" quantity; and A_{SR}, B_{SR}, C_{SR} and θ are the unknown parameters.

This condition equation is linearized by Taylor's expansion, and placed in the matrix form:

$$A_I V_I + B_I \Delta + \varepsilon_I^\circ = 0$$

in which

$$A_I = \left[\frac{\partial F_I}{\partial SR_I}\right] ,$$

V_I is the residual in SR_I,

$$B_I = \begin{bmatrix} \frac{\partial F_I}{\partial A_{SR}} & \frac{\partial F_I}{\partial B_{SR}} & \frac{\partial F_I}{\partial C_{SR}} & \frac{\partial F_I}{\partial \theta} \end{bmatrix},$$

$$\Delta = \begin{bmatrix} \delta A_{SR} \\ \delta B_{SR} \\ \delta C_{SR} \\ \delta \theta \end{bmatrix},$$ the vector of corrections to estimates of the unknown quantities,

and ε_I° is F_I evaluated using approximations for the unknown parameters.

The partial derivatives are evaluated as follows:

$$\frac{\partial F_I}{\partial SR_I} = -1$$

$$\frac{\partial F_I}{\partial A_{SR}} = 1$$

$$\frac{\partial F_I}{\partial B_{SR}} = r_I \cos \theta + t_I \sin \theta$$

$$\frac{\partial F_I}{\partial C_{SR}} = (r_I \cos \theta + t_I \sin \theta)^2$$

$$\frac{\partial F_I}{\partial \theta} = B_{SR}(t_I \cos \theta - r_I \sin \theta) +$$

$$+ 2C_{SR}(r_I \cos \theta + t_I \sin \theta)\ (t_I \cos \theta - r_I \sin \theta)$$

For n control points, the set of linearized condition equations for the least squares solution is:

$$A\ V + B\ \Delta + \varepsilon^{\circ} = 0$$

in which

$$A = I_n$$

$$V = \begin{bmatrix} V_1 \\ V_2 \\ \vdots \\ V_n \end{bmatrix}, \quad B = \begin{bmatrix} B_1 \\ B_2 \\ \vdots \\ B_n \end{bmatrix}, \text{ and } \varepsilon^{\circ} = \begin{bmatrix} \varepsilon_1^{\circ} \\ \varepsilon_2^{\circ} \\ \vdots \\ \varepsilon_n^{\circ} \end{bmatrix}.$$

The normal equations are:

$$B^T W B\ \Delta + B^T W \varepsilon^{\circ} = 0\ ,$$

in which

$$W = [A Q A^T]^{-1} = I_n\ ,$$

since $A = I_n$, and $Q = I_n$; i.e., the computed slant ranges are assumed independent and equal in precision.

The normal equations are solved for Δ:

$$\Delta = -\ (B^T W B)^{-1}\ B^T W \varepsilon^{\circ}$$

The solution is iterated with the parameter approximations being updated by the Δ corrections for each iteration. When $\Delta = 0$ or less than a predetermined convergence limit, the solution is completed.

The residuals, V, are then computed to determine how well the polynomial fits the given data.

Coefficients can be evaluated for each radar record, or the radar records can be combined to determine common values for B_{SR} and C_{SR}. In this case, the solution incorporates the data from all radar records, and an expanded set of condition equations is used.

3. TIME CORRELATION

The "time" polynomials for point I are:

$$X_{R_I} = A_X + B_X T_I + C_X T_I^2$$

$$Y_{R_I} = A_Y + B_Y T_I + C_Y T_I^2$$

$$Z_{R_I} = A_Z + B_Z T_I + C_Z T_I^2$$

in which X_{R_I}, Y_{R_I} and Z_{R_I} are the radar air station coordinates for the I^{th} ground point; and the plate coordinate, T_I, is computed as follows:

$$T_I = t_I \cos \theta - r_I \sin \theta \ .$$

The coefficients A_X, B_X, C_X, A_Y, B_Y, C_Y, A_Z, B_Z, and C_Z are evaluated using the method of least squares. For each control point, I, the three condition equations are:

$$F_{X_I} = A_X + B_X T_I + C_X T_I^2 - X_{R_I} = 0$$

$$F_{Y_I} = A_Y + B_Y T_I + C_Y T_I^2 - Y_{R_I} = 0$$

$$F_{Z_I} = A_Z + B_Z T_I + C_Z T_I^2 - Z_{R_I} = 0 \ .$$

These condition equations are already in linear form with respect to the unknown coefficients. Furthermore, with T_I fixed, and X_{R_I}, Y_{R_I} and Z_{R_I} as the "observed" quantities, the condition equations are independent, and thus can be treated separately.

In matrix form, with residuals, the X-equation is:

$$A_I V_I + B_I \Delta + \varepsilon_I^\circ = 0$$

in which

$$A_I = -1$$

V_I is the residual in X_{R_I},

$$B_I = [1 \quad T_I \quad T_I^{\,2}],$$

$$\Delta = \begin{bmatrix} A_X \\ B_X \\ C_X \end{bmatrix},$$

and

$$\varepsilon_I^\circ = -X_{R_I}.$$

For n control points, the set of n X-equations is:

$$\begin{bmatrix} -V_{1X} \\ -V_{2X} \\ \vdots \\ -V_{nX} \end{bmatrix} + \begin{bmatrix} 1 & T_1 & T_1^{\,2} \\ 1 & T_2 & T_2^{\,2} \\ & \cdots\cdots & \\ 1 & T_n & T_n^{\,2} \end{bmatrix} \begin{bmatrix} A_X \\ B_X \\ C_X \end{bmatrix} + \begin{bmatrix} -X_{R_1} \\ -X_{R_2} \\ \vdots \\ -X_{R_n} \end{bmatrix} = \begin{bmatrix} 0 \\ 0 \\ \vdots \\ 0 \end{bmatrix}$$

The normal equations are then:

$$\begin{bmatrix} n & \Sigma T_I & \Sigma T_I^{\,2} \\ \Sigma T_I & \Sigma T_I^{\,2} & \Sigma T_I^{\,3} \\ \Sigma T_I^{\,2} & \Sigma T_I^{\,3} & \Sigma T_I^{\,4} \end{bmatrix} \begin{bmatrix} A_X \\ B_X \\ C_X \end{bmatrix} = \begin{bmatrix} \Sigma X_{R_I} \\ \Sigma T_I \, X_{R_I} \\ \Sigma T_I^{\,2} \, X_{R_I} \end{bmatrix} .$$

These normal equations are solved for A_X, B_X and C_X. Similar solutions can be obtained for the Y-equations and the Z-equations.

4. RADAR RANGE INTERSECTION FOR POSITION

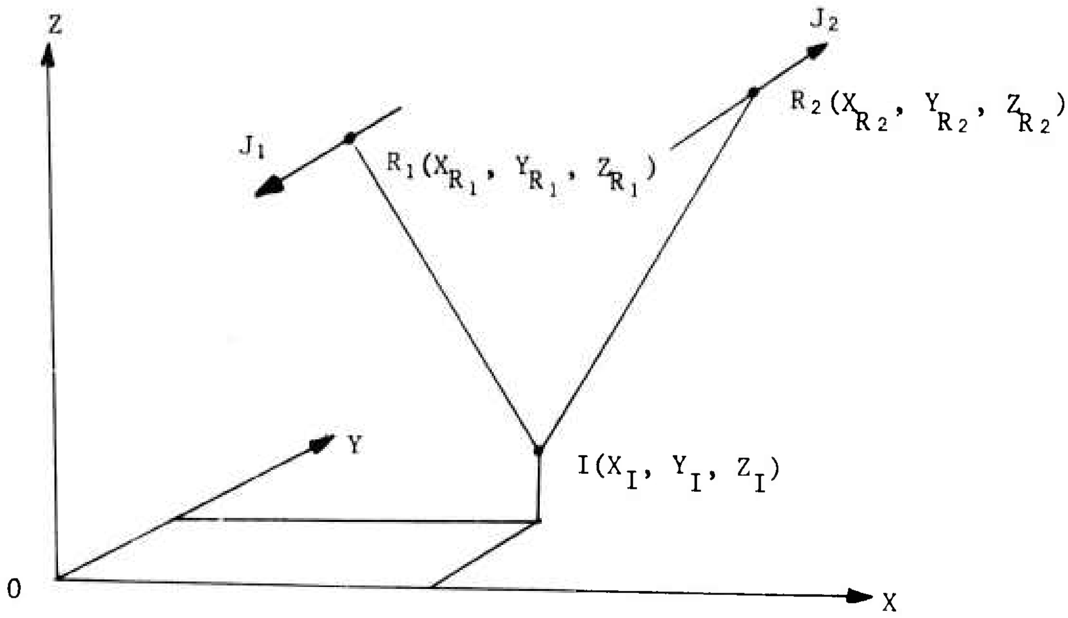

Figure A-2

Consider Figure A-2. J_1 and J_2 are two radar passes, each of which image ground point I on a radar record. Point R_1 on flight J_1 is the point in time along the flight path when ground point I is imaged on the radar record; i.e., at point R_1 the radar zero-Doppler line is perpendicular to the flight path and passes through ground point I. Two equations can be written from this situation:

1) Slant range equation.

$$(X_I - X_{R_1})^2 + (Y_I - Y_{R_1})^2 + (Z_I - Z_{R_1})^2 = SR^2_{I_1}$$

which gives the slant range from point R_1 to point I.

2) Equation of plane perpendicular to J_1 and through I.

$$\alpha_1(X_I - X_{R_1}) + \beta_1(Y_I - Y_{R_1}) + \gamma_1(Z_I - Z_{R_1}) = 0$$

where α_1, β_1, γ_1 are direction numbers for J_1 at the time of R_1.

Two similar equations can be written for J_2, resulting in a total of 4 equations in 3 unknowns (X_I, Y_I, Z_I).

$$F_{I_1} = SR_{I_1} - [(X_I - X_{R_1})^2 + (Y_I - Y_{R_1})^2 + (Z_I - Z_{R_1})^2]^{\frac{1}{2}} = 0$$

$$G_{I_1} = \alpha_1(X_I - X_{R_1}) + \beta_1(Y_I - Y_{R_1}) + \gamma_1(Z_I - Z_{R_1}) = 0$$

$$F_{I_2} = SR_{I_2} - [(X_I - X_{R_2})^2 + (Y_I - Y_{R_2})^2 + (Z_I - Z_{R_2})^2]^{\frac{1}{2}} = 0$$

$$G_{I_2} = \alpha_2(X_I - X_{R_2}) + \beta_2(Y_1 - Y_{R_2}) + \gamma_2(Z_I - Z_{R_2}) = 0 .$$

In the 4 derived equations, SR_{I_1} and SR_{I_2} are functions of image coordinates R_{I_1} and R_{I_2}; that is,

$$SR_{I_1} = A_{SR_1} + B_{SR_1} R_{I_1} + C_{SR_1} R_{I_1}^2$$

$$SR_{I_2} = A_{SR_2} + B_{SR_2} R_{I_2} + C_{SR_2} R_{I_2}^2;$$

and X_{R_1}, Y_{R_1}, Z_{R_1}, X_{R_2}, Y_{R_2} and Z_{R_2} are functions of image coordinates T_{I_1} and T_{I_2}; that is,

$$X_{R_1} = A_{X_1} + B_{X_1} T_{I_1} + C_{X_1} T_{I_1}^2$$

$$Y_{R_1} = A_{Y_1} + B_{Y_1} T_{I_1} + C_{Y_1} T_{I_1}^2$$

$$Z_{R_1} = A_{Z_1} + B_{Z_1} T_{I_1} + C_{Z_1} T_{I_1}^2$$

$$X_{R_2} = A_{X_2} + B_{X_2} T_{I_2} + C_{X_2} T_{I_2}^2$$

$$Y_{R_2} = A_{Y_2} + B_{Y_2} T_{I_2} + C_{Y_2} T_{I_2}^2$$

$$Z_{R_2} = A_{Z_2} + B_{Z_2} T_{I_2} + C_{Z_2} T_{I_2}^2 \quad .$$

Image coordinates R_{I_1}, T_{I_1}, R_{I_2}, and T_{I_2} are considered as observations. The unknown quantities are X_I, Y_I and Z_I.

The linearized equations in the general matrix form are:

$$A_I V_I + B_I \Delta_I + \varepsilon_I^\circ = 0 \ ,$$

where

A_I is a 4x4 coefficient matrix of partial derivatives of the condition equations with respect to the observations.

V_I is a 4×1 column vector of corrections to the unadjusted observations.

B_I is a 4×3 matrix of partial derivatives of the condition equations with respect to the unknown parameters.

Δ_I is a 3×1 column vector of corrections to the parameter approximations.

ε_I° is a 4×1 column vector of constants which are the condition equations evaluated for the approximate parameters.

Now,

$$A_I = \begin{bmatrix} \frac{\partial F_{I_1}}{\partial R_{I_1}} & \frac{\partial F_{I_1}}{\partial T_{I_1}} & 0 & 0 \\ \frac{\partial G_{I_1}}{\partial R_{I_1}} & \frac{\partial G_{I_1}}{\partial T_{I_1}} & 0 & 0 \\ 0 & 0 & \frac{\partial F_{I_2}}{\partial R_{I_2}} & \frac{\partial F_{I_2}}{\partial T_{I_2}} \\ 0 & 0 & \frac{\partial G_{I_2}}{\partial R_{I_2}} & \frac{\partial G_{I_2}}{\partial T_{I_2}} \end{bmatrix}$$

$$V_I = \begin{bmatrix} V_{R_{I_1}} \\ V_{T_{I_1}} \\ V_{R_{I_2}} \\ V_{T_{I_2}} \end{bmatrix}$$

$$B_I = \begin{bmatrix} \frac{\partial F_{I_1}}{\partial X_I} & \frac{\partial F_{I_1}}{\partial Y_I} & \frac{\partial F_{I_1}}{\partial Z_I} \\ \frac{\partial G_{I_1}}{\partial X_I} & \frac{\partial G_{I_1}}{\partial Y_I} & \frac{\partial G_{I_1}}{\partial Z_I} \\ \frac{\partial F_{I_2}}{\partial X_I} & \frac{\partial F_{I_2}}{\partial Y_I} & \frac{\partial F_{I_2}}{\partial Z_I} \\ \frac{\partial G_{I_2}}{\partial X_I} & \frac{\partial G_{I_2}}{\partial Y_I} & \frac{\partial G_{I_2}}{\partial Z_I} \end{bmatrix}$$

$$\Delta_I = \begin{bmatrix} \Delta X_I \\ \Delta Y_I \\ \Delta Z_I \end{bmatrix} \quad \text{and} \quad \varepsilon_I^\circ = \begin{bmatrix} F^\circ_{I_1} \\ G^\circ_{I_1} \\ F^\circ_{I_2} \\ G^\circ_{I_2} \end{bmatrix}$$

For the A_I matrix, the partial derivatives of F_{I_1} and F_{I_2} are:

$$\frac{\partial F_{I_1}}{\partial R_{I_1}} = \frac{\partial F_{I_1}}{\partial SR_{I_1}} \cdot \frac{\partial SR_{I_1}}{\partial R_{I_1}}$$

$$\frac{\partial F_{I_2}}{\partial R_{I_2}} = \frac{\partial F_{I_2}}{\partial SR_{I_2}} \cdot \frac{\partial SR_{I_2}}{\partial R_{I_2}} ,$$

$$\frac{\partial F_{I_1}}{\partial T_{I_1}} = \frac{\partial F_{I_1}}{\partial X_{R_1}} \cdot \frac{\partial X_{R_1}}{\partial T_{I_1}} + \frac{\partial F_{I_1}}{\partial Y_{R_1}} \cdot \frac{\partial Y_{R_1}}{\partial T_{I_1}} + \frac{\partial F_{I_1}}{\partial Z_{R_1}} \cdot \frac{\partial Z_{R_1}}{\partial T_{I_1}} ,$$

$$\frac{\partial F_{I_2}}{\partial T_{I_2}} = \frac{\partial F_{I_2}}{\partial X_{R_2}} \cdot \frac{\partial X_{R_2}}{\partial T_{I_2}} + \frac{\partial F_{I_2}}{\partial Y_{R_2}} \cdot \frac{\partial Y_{R_2}}{\partial T_{I_2}} + \frac{\partial F_{I_2}}{\partial Z_{R_2}} \cdot \frac{\partial Z_{R_2}}{\partial T_{I_2}} ,$$

from which

$$\frac{\partial F_{I_1}}{\partial R_{I_1}} = 2(A_{SR_1} + B_{SR_1} R_{I_1} + C_{SR_1} R_{I_1}^2)(B_{SR_1} + 2C_{SR_1} R_{I_1})$$

$$\frac{\partial F_{I_2}}{\partial R_{I_2}} = 2(A_{SR_2} + B_{SR_2} R_{I_2} + C_{SR_2} R_{I_2}^2)(B_{SR_2} + 2C_{SR_2} R_{I_2})$$

$$\frac{\partial F_{I_1}}{\partial T_{I_1}} = \frac{1}{SR_{I_1}} \Big[(X_I - X_{R_1})(B_{X_1} + 2C_{X_1} T_{I_1}) + (Y_I - Y_{R_1})(B_{Y_1} + 2C_{Y_1} T_{I_1}) + + (Z_I - Z_{R_1})(B_{Z_1} + 2C_{Z_1} T_{I_1}) \Big]$$

$$\frac{\partial F_{I_2}}{\partial T_{I_2}} = \frac{1}{SR_{I_2}} \Big[(X_I - X_{R_2})(B_{X_2} + 2C_{X_2} T_{I_2}) + (Y_I - Y_{R_2})(B_{Y_2} + 2C_{Y_2} T_{I_2}) + + (Z_I - Z_{R_2})(B_{Z_2} + 2C_{Z_2} T_{I_2}) \Big]$$

Similarly, the partial derivatices of G_{I_1} and G_{I_2} are:

$$\frac{\partial G_{I_1}}{\partial R_{I_1}} = \frac{\partial G_{I_2}}{\partial R_{I_2}} = 0 ,$$

and

$$\frac{\partial G_{I_1}}{\partial T_{I_1}} = - \alpha_1 (B_{X_1}+2C_{X_1} \; T_{I_1}) - \beta_1 (B_{Y_1}+2C_{Y_1} \; T_{I_1}) - \gamma_1 (B_{Z_1}+2C_{Z_1} \; T_{I_1})$$

$$\frac{\partial G_{I_2}}{\partial T_{I_2}} = - \alpha_2 (B_{X_2}+2C_{X_2} \; T_{I_2}) - \beta_2 (B_{Y_2}+2C_{Y_2} \; T_{I_2}) - \gamma_2 (B_{Z_2}+2C_{Z_2} \; T_{I_2}) .$$

The required partial derivatives for the B_I matrix are:

$$\frac{\partial F_{I_1}}{\partial X_I} = \frac{(X_I-X_{R_1})}{SR_{I_1}} , \quad \frac{\partial F_{I_2}}{\partial X_I} = \frac{(X_I-X_{R_2})}{SR_{I_2}}$$

$$\frac{\partial F_{I_1}}{\partial Y_I} = \frac{(Y_I-Y_{R_1})}{SR_{I_1}} , \quad \frac{\partial F_{I_2}}{\partial Y_I} = \frac{(Y_I-Y_{R_1})}{SR_{I_2}}$$

$$\frac{\partial F_{I_1}}{\partial Z_I} = \frac{(Z_I-Z_{R_1})}{SR_{I_1}} , \quad \frac{\partial F_{I_2}}{\partial Z_I} = \frac{(Z_I-Z_{R_2})}{SR_{I_2}}$$

$$\frac{\partial G_{I_1}}{\partial X_I} = \alpha_1 , \quad \frac{\partial G_{I_2}}{\partial X_I} = \alpha_2$$

$$\frac{\partial G_{I_1}}{\partial Y_I} = \beta_1 , \quad \frac{\partial G_{I_2}}{\partial Y_I} = \beta_2$$

$$\frac{\partial G_{I_1}}{\partial Z_I} = \gamma_1 , \quad \frac{\partial G_{I_2}}{\partial Z_I} = \gamma_2$$

The least squares solution is as follows:

The weight matrix W is

$$W_I = (A_I \sigma_I A_I^T)^{-1}$$

where

$$\sigma_I = \begin{bmatrix} \sigma^2_{R_{I_1}} & & & 0 \\ & \sigma^2_{T_{I_1}} & & \\ & & \sigma^2_{R_{I_2}} & \\ 0 & & & \sigma^2_{T_{I_2}} \end{bmatrix}$$

in which the σ^2's are the estimated variances of the image coordinates.

The correction vector Δ_I is computed from the matrix equation

$$\Delta_I = \begin{bmatrix} \Delta X_I \\ \Delta Y_I \\ \Delta Z_I \end{bmatrix} = -(B_I^T W_I B_I)^{-1} B_I^T W_I \varepsilon_I^\circ$$

The solution is iterated with the parameter approximations being updated by the Δ corrections for each iteration. When $\Delta = 0$ or is less than a predetermined convergence limit, the solution is completed.

A statistical analysis of the solution can be performed by making the following computations:

The vector V_I is computed from

$$V_I = -(\sigma_I A_I^T W_I)^{-1} (B_I \Delta_I + \varepsilon_I^\circ)$$

$V_I^T \sigma_I V_I$ is computed directly, or from $V_I^T \sigma_I V_I = \varepsilon_I^{\circ T} W_I \varepsilon_I^\circ$.

The a posteriori variance of unit weight $\hat{\sigma}^2_{\circ I}$ can then be found from

$$\hat{\sigma}^2_{\circ I} = \frac{V_I^T \sigma_I^{-1} V_I}{M - P}$$

where M is the number of condition equations and P is the number of unknown parameters.

The covariance matrix for the unknown parameters can be estimated from

$$\text{cov } \Delta_I = \hat{\sigma}^2_{\circ I} (B_I^T W_I B_I)^{-1} .$$

Unclassified

Security Classification

DOCUMENT CONTROL DATA - R&D

(Security classification of title, body of abstract and indexing annotation must be entered when the overall report is classified)

1 ORIGINATING ACTIVITY (Corporate author) Raytheon Company Equipment Division Autometric Operation	2a. REPORT SECURITY CLASSIFICATION Unclassified 2b GROUP

3 REPORT TITLE

Stereo Radar Analysis

4 DESCRIPTIVE NOTES (Type of report and inclusive dates)

Final Technical Report, March 1969 to April 1970

5 AUTHOR(S) (Last name, first name, initial)

Gracie, Gordon — Bricker, John W.
Brewer, Ronald K. — Johnson, Robert A.

6 REPORT DATE	7a. TOTAL NO. OF PAGES	7b. NO. OF REFS
May 1970	83	2

8a CONTRACT OR GRANT NO DACA76-69-C-0002 b PROJECT NO c ARPA Order No. 1229 d Program Code No. 8F40	9a. ORIGINATOR'S REPORT NUMBER(S) FTR-1339-1 9b. OTHER REPORT NO(S) (Any other numbers that may be assigned this report)

Distribution limited to U.S. Government agencies only: test and evaluation; Sep 72. Other requests for this document must be referred to Commanding Officer, U.S. Army Engineer Topographic Labs. ATTN: ETL-TDL, Ft. Belvoir, Va. 22060

11 SUPPLEMENTARY NOTES	12. SPONSORING MILITARY ACTIVITY
	Advanced Research Projects Agency (ARPA) Washington, D. C.

13 ABSTRACT The topographic accuracy of the AN/APQ-102(XA-2) side-looking radar and its specific applicability to 1:50,000 and 1:250,000 scale topographic mapping were tested using stereo radar techniques with real data. The two basic stereo configurations, opposite-side and same-side, were tested. Also tested was the geometric fit of each individual radar record to the established ground control. Although original plans called for a test area 25 miles long by 4 miles wide, shortcomings in the data actually acquired led to adoption of a much smaller test area. Moreover, lack of certain collateral data required development of a special reduction technique based upon ground control in the test area. Photogrammetric aerotriangulation of aerial photography flown simultaneously with the radar provided a means of defining the flight path. Ground points in the test area were also aerotriangulated, and used as control and as the standard for measuring radar accuracy. The test results were surprisingly good, with the opposite-side stereo configuration providing the better accuracy. Average root mean square (RMS) values of 7.7 meters, 12.1 meters and 13.2 meters in X(across-track), Y(along-track) and Z(elevation), respectively, were obtained for the opposite-side case; corresponding RMS values of 9.5 meters, 20.0 meters and 16.7 meters were obtained for the same-side case. Results from fitting the individual radar records to the aerotriangulated positions also demonstrated excellent geometric fidelity in the radar imagery. Although based upon limited data, the test results indicate that the AN/APQ-102(XA-2) radar, using stereo techniques, has much promise for all-weather, day-night mapping at scales of 1:50,000 and 1:250,000.

DD FORM 1 JAN 64 1473

Unclassified

Security Classification

Unclassified

Security Classification

14. KEY WORDS	LINK A ROLE	LINK A WT	LINK B ROLE	LINK B WT	LINK C ROLE	LINK C WT
Side-looking Radar						
Stereo Radar						
Topographic Accuracy						
Geometric Fidelity						
Radar Mensuration						
Aerotriangulation						

INSTRUCTIONS

1. ORIGINATING ACTIVITY: Enter the name and address of the contractor, subcontractor, grantee, Department of Defense activity or other organization *(corporate author)* issuing the report.

2a. REPORT SECURITY CLASSIFICATION: Enter the overall security classification of the report. Indicate whether "Restricted Data" is included. Marking is to be in accordance with appropriate security regulations.

2b. GROUP: Automatic downgrading is specified in DoD Directive 5200.10 and Armed Forces Industrial Manual. Enter the group number. Also, when applicable, show that optional markings have been used for Group 3 and Group 4 as authorized.

3. REPORT TITLE: Enter the complete report title in all capital letters. Titles in all cases should be unclassified. If a meaningful title cannot be selected without classification, show title classification in all capitals in parenthesis immediately following the title.

4. DESCRIPTIVE NOTES: If appropriate, enter the type of report, e.g., interim, progress, summary, annual, or final. Give the inclusive dates when a specific reporting period is covered.

5. AUTHOR(S): Enter the name(s) of author(s) as shown on or in the report. Enter last name, first name, middle initial. If military, show rank and branch of service. The name of the principal author is an absolute minimum requirement.

6. REPORT DATE: Enter the date of the report as day, month, year, or month, year. If more than one date appears on the report, use date of publication.

7a. TOTAL NUMBER OF PAGES: The total page count should follow normal pagination procedures, i.e., enter the number of pages containing information.

7b. NUMBER OF REFERENCES: Enter the total number of references cited in the report.

8a. CONTRACT OR GRANT NUMBER: If appropriate, enter the applicable number of the contract or grant under which the report was written.

8b, 8c, & 8d. PROJECT NUMBER: Enter the appropriate military department identification, such as project number, subproject number, system numbers, task number, etc.

9a. ORIGINATOR'S REPORT NUMBER(S): Enter the official report number by which the document will be identified and controlled by the originating activity. This number must be unique to this report.

9b. OTHER REPORT NUMBER(S): If the report has been assigned any other report numbers *(either by the originator or by the sponsor)*, also enter this number(s).

10. AVAILABILITY/LIMITATION NOTICES: Enter any limitations on further dissemination of the report, other than those imposed by security classification, using standard statements such as:

(1) "Qualified requesters may obtain copies of this report from DDC."

(2) "Foreign announcement and dissemination of this report by DDC is not authorized."

(3) "U. S. Government agencies may obtain copies of this report directly from DDC. Other qualified DDC users shall request through ______________________."

(4) "U. S. military agencies may obtain copies of this report directly from DDC. Other qualified users shall request through ______________________."

(5) "All distribution of this report is controlled. Qualified DDC users shall request through ______________________."

If the report has been furnished to the Office of Technical Services, Department of Commerce, for sale to the public, indicate this fact and enter the price, if known.

11. SUPPLEMENTARY NOTES: Use for additional explanatory notes.

12. SPONSORING MILITARY ACTIVITY: Enter the name of the departmental project office or laboratory sponsoring *(paying for)* the research and development. Include address.

13. ABSTRACT: Enter an abstract giving a brief and factual summary of the document indicative of the report, even though it may also appear elsewhere in the body of the technical report. If additional space is required, a continuation sheet shall be attached.

It is highly desirable that the abstract of classified reports be unclassified. Each paragraph of the abstract shall end with an indication of the military security classification of the information in the paragraph, represented as *(TS), (S), (C), or (U)*

There is no limitation on the length of the abstract. However, the suggested length is from 150 to 225 words.

14. KEY WORDS: Key words are technically meaningful terms or short phrases that characterize a report and may be used as index entries for cataloging the report. Key words must be selected so that no security classification is required. Identifiers, such as equipment model designation, trade name, military project code name, geographic location, may be used as key words but will be followed by an indication of technical context. The assignment of links, rules, and weights is optional.

End- 10-72

Unclassified

Security Classification